HAL
open science

Oceanic factors controlling the Indian summer monsoon onset in a coupled model

Chloé Prodhomme, Pascal Terray, Sébastien Masson, Ghyslaine Boschat, Takeshi Izumo

1   <u>Oceanic factors controlling the Indian summer monsoon onset in a coupled model</u>

2

3

4   Chloé Prodhomme[1], Pascal Terray[1,2], Sébastien Masson[1], Ghyslaine Boschat[1], Takeshi Izumo[1]

5

6

7

8   [1]Sorbonne Universites (UPMC, Univ Paris 06)-CNRS-IRD-MNHN, LOCEAN

9   Laboratory, 4 place Jussieu, F-75005 Paris, France

10   [2] Indo-French Cell for Water Sciences, IISc-NIO-IITM–IRD Joint International

11   Laboratory, IITM, Pune, India

12

13

14

15

16

19

20

21

22

23

24   Corresponding author address: Chloé Prodhomme

25   Institut Català de Ciències del Clima

26   Doctor Trueta, 203 - 08005 Barcelona, Spain

27

28   E-mail: chloe.prodhomme@locean-ipsl.upmc.fr

29 **<u>Abstract</u>**

30 *Despite huge socio-economical impacts, the predictability of the Indian Summer Monsoon (ISM)*

31 *onset remains drastically limited by the inability of both current forced and coupled models to*

32 *reproduce a realistic monsoon seasonal cycle. In the SINTEX-F2 coupled model, the mean ISM onset*

33 *estimated with rainfall or thermo-dynamical indices is delayed by approximately 13 days, but it*

34 *occurs 6 days early in the atmosphere-only component of the coupled model. This 19 days lag between*

35 *atmospheric-only and coupled runs, which is well above the observed standard-deviation of the ISM*

36 *onset (10 days in the observations), suggests a crucial role of the coupling, including Sea Surface*

37 *Temperatures (SST) biases, on the delayed mean onset in the coupled model.*

38 *On the other hand, the key-factors governing the interannual variability of the ISM onset date are*

39 *also fundamentally different in the atmospheric and coupled experiments and highlight the*

40 *importance of El Niño–Southern Oscillation (ENSO) and ocean-atmosphere coupling for a realistic*

41 *simulation of the variability of the ISM onset date.*

42 *At both interannual and seasonal timescales, we demonstrate the importance of the meridional*

43 *gradients of tropospheric temperature, moisture and vertical shear of zonal wind in the Indian Ocean*

44 *for a realistic ISM onset simulation. Taking into account that the tropical tropospheric temperature*

45 *and the vertical shear are not only controlled by local processes, but also by large-scale processes, we*

46 *need to examine not only the Indian Ocean SST biases, but also those in others tropical basins in*

47 *order to understand the delay of the mean onset date in the coupled model. During April and May, the*

48 *main tropical SST biases in the coupled model are a strong warm bias in the Indian, Pacific and*

49 *Atlantic oceans, associated with an important excess of equatorial precipitations, and thus a warmer*

50 *equatorial free troposphere.*

51 *In order to identify the keys tropical SST regions influencing the mean ISM onset date, sensitivity*

52 *coupled experiments have been performed. In these experiments, the SST is corrected separately in*

53 *each tropical basin. The correction of SST biases in the tropical Indian and Atlantic oceans only*

54 *slightly improves the onset date in the coupled model and produces "El Niño-like" changes in the*

55 *tropical Pacific. Conversely, the correction of the Pacific SST biases advances the onset date by 9*

56 *days compared to the control coupled run. These results suggest that, while the correction of Indian*

57 *SST biases improves the rainfall spatial distribution, the delayed mean ISM onset date is mainly*

58   *control by the tropical Pacific Ocean SST biases.*

59

1. Introduction

The Indian Summer Monsoon (ISM) is one of the most dominant tropical atmospheric circulations, and the economies and livelihood of the populations of India depend heavily on its rainfall (see the reviews in Webster et al., 1998; Goswami, 2005a; Wang, 2006). The ISM onset refers to the sudden rise of rainfall over India between the end of May and mid-July depending on the regions, after a dry period of 6 months over most of the Indian subcontinent (Ananthakrishnan and Soman, 1988). The ISM begins over Kerala before moving progressively northward to reach the foothills of Himalaya in late June (Wang and LinHo, 2002). Despite of its low interannual variability (standard deviation of about 10 days), determining the ISM onset date is crucial for agriculture since deficiency of rainfall at the beginning of the rainy season can result in reduced crop yields, especially for the crops planted in anticipation of the ISM rainfall. Advanced and accurate forecast of the ISM onset date has thus significant societal applications.

On a scientific basis, a first important question is whether the ISM onset has higher predictability than daily rainfall variability and this seems to be the case since some statistical and dynamical models exhibit significant skill in predicting the ISM onset date with a lead time of up to around 15 to 30 days (Vitard and Molteni, 2009; Pai and Rajeevan, 2009; Gouda and Goswami, 2010). This suggests that the ISM onset is a large-scale transition in the monsoon seasonal cycle primarily driven by regional and large-scale circulations in which synoptic noise plays a secondary role (Ananthakrishnan and Soman, 1988; Joseph et al., 1994, 2006; Wang et al., 2009).

However, the ISM onset remains a complex and challenging phenomenon, governed by a number of processes at different spatial and temporal scales (Webster, 1983; Li and Yanai, 1996; He et al., 2003; Minoura et al. 2003; Wang et al. 2009; Lau and Nath, 2012, among many others). First, many studies have shown the importance of the Tibetan Plateau as an elevated heat source for the establishment of the ISM circulation (Flohn, 1957; Yanai et al., 2002; He et al., 2003; Sato and Kimura, 2007; Abe et al., 2013; Rajagopalan and Molnar, 2013). As an illustration, Li and Yanai (1996), He et al. (2003) and Xavier et al. (2007) have demonstrated that the ISM onset date, as estimated from rainfall observations, is in phase with the reversal of the meridional tropospheric

90   temperature gradient just south of the Tibetan Plateau. Dai et al. (2013) have further confirmed
91   that the upper tropospheric temperature plays a bigger role than the surface temperature driving
92   the monsoon circulation. The physical mechanism underlying the links between the thermal
93   contrasts at upper levels and the intensity of monsoon circulation can be understood in the
94   framework of the thermal wind equations (Dai et al., 2013). Others studies have highlighted the
95   role of different parameters, such as hydrology (Webster, 1983; Rajendran et al., 2002), snow cover
96   (Vernekar et al., 1995; Bamzai and Shukla, 1999; Bamzai and Marx, 2000) or vegetation
97   (Yamashima et al., 2011).

98

99   The ISM onset over Kerala and its subsequent northward progression at higher latitudes can also
100   be interpreted as the first episode of the northward propagating IntraSeasonal Oscillations (ISOs)
101   in the Indian region (Krishnamurti, 1985; Webster et al., 1998; Goswami, 2005b). Nevertheless,
102   Lee et al. (2013) have recently suggested that the ISM onset is more tightly linked to the biweekly
103   mode of intraseasonal variability than the canonical northward propagating ISOs with a 30-60
104   days periodicity.

105

106   Another controversial matter is the relationship between ISM and tropical Sea Surface
107   Temperatures (SST). Both observational and modeling studies have proved that the ISM and its
108   onset are strongly influenced by the El Niño–Southern Oscillation (ENSO) phenomenon (Joseph et
109   al., 1994; Soman and Slingo, 1997; Annamalai et al., 2005; Xavier et al., 2007; Boschat et al., 2011;
110   Lau and Nath, 2012 among many others). However, the role of Indian Ocean SSTs on the ENSO-
111   monsoon system is not fully understood. Many studies have highlighted the crucial role of coupling
112   processes over the Indian Ocean for a realistic ISM simulation and a proper ENSO teleconnection
113   (Wang et al., 2005; Krishna Kumar et al., 2005; Wu and Kirtman, 2004, 2007; Krishnan et al.,
114   2010). In line with these studies, different authors have suggested that the Indian Ocean SSTs may
115   influence the ISM onset date, especially the Arabian Sea warm pool (Masson et al., 2005; Sijikumar
116   and Rajeev, 2012) or the southwest Indian Ocean (Joseph et al., 1994; Annamalai et al., 2005;
117   Boschat et al., 2011). Conversely, a few studies have found no coherent relationship between ISM
118   onset and Indian Ocean SSTs (Shukla, 1987; Li and Yanai, 1996; Prodhomme et al., 2014). Thus, it
119   appears essential to better assess the respective role of Indian and Pacific oceans SSTs on the ISM
120   onset. Finally, there is also evidence of an association between the variability of Atlantic SSTs and

121 the early part of ISM (Kucharski et al., 2008). In other words, assessing the influence of Indian,

122 Pacific and Atlantic oceans SSTs on the ISM onset is still an open problem.

123

124 Despite of its societal significance, our current ability to simulate the ISM onset date is still quite

125 low in both Atmospheric General Circulation Models (AGCMS) and Coupled General Circulation

126 Models (CGCMs). Some AGCMs are able to reproduce a realistic onset date (Cherchi and Navarra,

127 2003; Annamalai et al, 2005; Ratna et al., 2011). However, in their comparison of 11 AGCMS, Wang

128 et al. (2004) show that all these models tend to overestimate precipitation over India during the

129 pre-monsoon and monsoon seasons, which implies a too early onset. In CGCMs, the onset date

130 simulation is not any more successful, with many CGCMs simulating a delayed ISM onset: Kripalani

131 et al. (2007) show that only 7 of 22 models submitted to the World Climate Research Program's

132 (WCRP) Coupled Model Intercomparison Project (CMIP) phase 3 are able to reproduce the abrupt

133 seasonal changes in the precipitation annual cycle over India. Zhang et al. (2012) and Sperber et al.

134 (2013) obtain similar conclusions with the CMIP5 CGCMs. The overall deficiencies of AGCMs and

135 CGCMs to reproduce the mean state and variability in the Indian areas, as well as the ENSO-

136 monsoon relationship, could partly explain the inability of current state of the art models to

137 simulate the ISM onset (Terray et al., 2012; Prodhomme et al., 2014).

138

139 However, to the best of our knowledge, no quantitative assessment of the respective merits and

140 caveats of AGCMs versus CGCMs for the simulation of the ISM onset has so far been made. Since

141 ENSO teleconnections and monsoon ISOs, which are associated with the ISM onset, are better

142 resolved by CGCMs (Wang et al., 2005; Fu et al. 2003, 2007; Fu and Wang, 2004; Rajendran and

143 Kitoh, 2006; Woolnough et al., 2007; Klingaman et al., 2011), it would be interesting to compare

144 the performance of AGCMs and CGCMs in simulating the ISM onset. A second objective of the

145 paper is to show the results obtained with several sensitivity experiments, which were designed to

146 delineate how the simulated mean state in each oceanic basin impacts the ISM onset in a CGCM.

147 Despite our recognition of the influences of SST in each oceanic basin, as outlined above, the

148 relative contribution of each basin to the mean and variability of the ISM onset date has not been

149 assessed comprehensively in a modeling framework.

150

151 The paper is organized as follows. The validation datasets, the coupled model, and the design of the

sensitivity experiments are described in Section 2. The method used to define the ISM onset is discussed in Section 3. In Section 4, we compare the mean state during the pre-monsoon period in observations, forced and coupled experiments. Section 5 details the variability of the ISM onset and its relationship with its possible oceanic precursors; and demonstrates the importance of the ocean-atmosphere coupling. Section 6 discusses results from the sensitivity experiments, and Section 7 summarizes the main results from this paper.

2. Description of Model and datasets

2.1 SINTEX-F2 model

We have used the standard configuration of the SINTEX-F2 model (Masson et al., 2012). It is the upgraded version of SINTEX-F1 CGCM (Guilyardi et al., 2003; Luo et al., 2003, 2005). The oceanic component is NEMO (Madec, 2008), using the ORCA05 horizontal resolution (0.5°), 31 vertical levels and including the LIM2 ice model (Timmermann et al., 2005). The atmospheric component is ECHAM 5.3 (Roeckner et al., 2003, 2004) with the T106 (1.125°) horizontal resolution, which corresponds to about 120 km, and 31 hybrid sigma-pressure levels. A mass flux scheme (Tiedtke, 1989) is applied for cumulus convection with modifications for penetrative convection according to Nordeng (1994). The coupling informations, without any flux corrections, are exchanged every 2 h by means of the OASIS 3 coupler (Valcke, 2006). See Masson et al. (2012) for further details.

We run a 110-years control experiment (named CTL hereafter) with the coupled configuration of SINTEX-F2. At the same time, we have run an AGCM experiment (named FOR hereafter) with the atmospheric-only configuration of SINTEX-F2, forced by Advanced Very High Resolution Radiometer (AVHRR) daily SST from 1982 to 2010, in order to assess the impact of the ocean-atmosphere coupling on the simulated statistics (mean and variability) of the ISM onset date. The performance of the SINTEX-F2 model in simulating the seasonal cycle in the Indian areas has been assessed in Prodhomme et al. (2014) and is not repeated here.

2.2 Design of the sensitivity experiments

In order to investigate the impact of SST biases in each ocean basin and to delineate the relative role of each basin in controlling the ISM onset date statistics (mean and variability), we performed 3 sensitivity-coupled experiments (named FTIO, FTA and FTP hereafter), where the

183 SST is corrected in each basin separately. A strong SST nudging is applied in the entire tropical
184 Indian, Atlantic and Pacific oceans in the FTIO, FTA and FTP experiments, respectively (see table
185 1). The simulations have a length of 50 years. For these experiments, we used the standard
186 configuration of the CGCM described previously without any flux corrections, except in the
187 corrected area where, following Luo et al. (2005), we applied a large feedback value (-2400 W.m^{-}
188 ^{2}.K^{-1}) to the surface heat flux. This value corresponds to the 1-day relaxation time for temperature
189 in a 50-m mixed layer. The SST damping is applied towards a daily climatology computed from
190 the AVHRR only daily Optimum Interpolation SST (OISST) version 2 dataset for the 1982-2010
191 period (Reynolds et al., 2007). A Gaussian smoothing is applied in a transition zone of 5° in both
192 longitude and latitude at the limits of the SST restoring domains. This large correction, using daily
193 climatology, fully corrects the SST biases and suppresses the SST variability in each corrected
194 region. It is important to keep in mind that the focus with these experiments is to delineate, at
195 the first order, how the SST biases in these regions impact the mean ISM onset date only. We
196 assumed that the impact of the suppressed variability in each corrected region is negligible
197 compared to the importance of the biases as far as the mean onset date is concerned.
198
199 In order to further clarify the role of the interannual SST variability of the Pacific Ocean, a fourth
200 sensitivity experiment has been run with a SST nudging applied in the tropical Pacific Ocean
201 toward a daily climatology computed from CTL instead of observations (called FTPC hereafter).
202 Thus, in this experiment there is no change in the Pacific SST mean state, but the Pacific SST
203 interannual variability is suppressed. The FTPC experiment has a duration of 30 years.
204
205 The details of each experiment are given in Table 1.
206
207 **2.3 Reference datasets**
208 For a comparison of rainfall between observations and the model outputs, we used the Tropical
209 Rainfall Measuring Mission (TRMM) observations, specifically the 0.25° by 0.25° horizontal
210 resolution merged 3B43 dataset, which is available from 1998 to 2010 (Kummerow et al., 2001;
211 Huffman et al., 1997). Winds, atmospheric temperature at different levels and precipitation from
212 the ERA-Interim reanalysis for the 1989-2009 period have also been used (Dee et al., 2011). For
213 SST, we used the AVHRR infrared satellite SST product from 1982 to 2010 (Reynolds et al., 2007).

214

3. Estimation of the ISM onset

216

217 To be able to study the ISM onset, an objective and precise definition is necesary. A large number of
218 methods have been proposed in the past to identify the ISM onset based on different variables
219 (rainfall, lower and upper level winds, vertically integrated moisture transport, temperature
220 gradient, etc.) and large disagreements can arise when comparing the ISM onset dates estimated
221 by the various methods (Ananthakrishnan and Soman, 1988; Joseph et al. al., 1994, 1996; Fasullo
222 and Webster, 2003; Taniguchi and Koike, 2006, Pai and Rajeevan, 2009; Wang et al., 2009). This
223 means that we must adopt one and only one method for defining the ISM onset in observations,
224 forced and coupled simulations in order to derive meaningful results.

225

226 The Indian Meteorological Department (IMD) has estimated the mean Monsoon Onset date over
227 Kerala (MOK) for more than 100 years with a help of a (subjective) method based on rain-gauge
228 rainfall estimations (Ananthakrishnan and Soman, 1988; Pai and Rajeevan, 2009). The current
229 definition states that the onset is declared after 2 days of precipitation exceeding 2.5 mm in Kerala
230 stations (Pai and Rajeevan, 2009). Wind and Outgoing Longwave Radiation (OLR) fields are also
231 taken into account to screen out "false" or "bogus" onsets as much as possible (Flatau et al., 2001;
232 Taniguchi and Koike, 2006, Pai and Rajeevan, 2009; Wang et al., 2009). The IMD established that
233 MOK is occurring on the 1st of June, with a standard deviation of 8 days. Nevertheless, as illustrated
234 on Figure 1a, the raw precipitation seasonal cycle is already extremely noisy and may vary in
235 AGCM versus CGCM simulations. Besides, the existence of "bogus" onsets further complicates the
236 matter of diagnosing objectively the ISM onset from rainfall time series (Fasullo and Webster,
237 2003; Wang et al., 2009). Thus, we suggest that the conventional set of criteria based on in-situ
238 rainfall is not best suited for determining the ISM onset in climate model simulations. Due to their
239 coarse-resolution and their current limited skill in simulating ISM rainfall, a larger scale and
240 dynamical method could be preferable to define objectively the ISM onset in climate simulations.

241

242 It is well known that the establishment and evolution of ISM is closely related to the evolution of
243 Tropospheric Temperature (TT, defined as the temperature averaged between 600 and 200 hPa)
244 and, more precisely to the change of sign of the meridional TT gradient between the south

equatorial and north Indian oceans, including India (Xavier et al., 2007; Dai et al., 2013). This gradient is governed by the evolution of the heat sources and sinks in this region (Yanai et al., 1992; Li and Yanai, 1996; He et al., 2003). Based on this evidence, Xavier et al. (2007) proposed an evaluation of the ISM onset date using this TT Gradient (TTG), which they defined as the difference of TT between a northern box (40°-100°E; 5°-35°N) and a southern box (40°-100°E; 15°S-5°N), as displayed in Figure 2. Figure 1b shows the seasonal cycle of this TTG index in observations, CTL and FOR experiments, and its comparison with Figure 1a demonstrates the close relationship between ISM precipitation and TTG. This relationship will be more thoroughly assessed in the next section. The ISM onset is then defined when the value of TTG changes sign from negative to positive and vice-versa for the withdrawal of ISM. The intensity of the monsoon may be estimated by the cumulative positive values of the TTG. These physically based definition of the ISM onset and intensity do not depend on an arbitrary threshold of precipitation and are less susceptible to "bogus" onsets, because they are based on large-scale indices and the slow variability of TT in the region. Moreover, Figure 1 shows that the TTG onset occurs approximately when precipitation exceeds 5mm/day, which is consistent with the onset estimation of Wang and LinHo (2002). Furthermore, the correlation between the observed TTG onset and IMD MOK is high and significant (0.61; Xavier et al., 2007). Figures 1a and b suggest that the ISM onset is strongly delayed in CTL compared to both FOR and observations. Figure 1a suggests also that, in FOR, the onset based on rainfall estimates seems simultaneous with observations, while it seems to occur earlier when using the TTG definition (Fig. 1b).

The observed ISM onset estimated with the TTG index occurs around the 29th of May, in good agreement with the MOK, while it occurs 6 days earlier in FOR and 13 days later in CTL. This 6 days difference between observations and FOR is not significant at the 90% confidence level, whereas the differences of CTL with both observations and FOR are well above the 99% confidence level (statistical significance of the differences computed with a Student's two-tailed t-test). The 19 days delay between FOR and CTL clearly suggests an important impact of coupling, especially of SST biased mean state (Prodhomme et al., 2014) and variability on the ISM onset, which warrants further investigation.

4. The pre-onset mean state

276

In this section, we first describe the surface temperature and TT patterns in FOR, CTL and observations during the pre-monsoon period. Then, we investigate the daily evolution of precipitation, TT and vertical shear of zonal wind (defined as the difference in zonal winds between 200 minus 850 hPa levels) over the Indian Ocean and their relationships with the ISM onset (derived from the TTG index). We also compare the global observed and simulated TT patterns during the pre-monsoon period in order to understand the differences between simulated and observed ISM onsets. Finally, the role of ISOs in the ISM onset and the differences between observations, FOR and CTL in various background state variables such as the zonal wind shear or specific humidity fields, which are key-elements for the northward propagation of the ISOs (Jiang et al., 2004), are analyzed. Our analysis focuses mainly on the period between the April 15th and the May 15th, in order to study the signals preceding the ISM onset, but avoiding the onset signal itself.

4.1 Tropospheric temperature gradient and land-sea thermal contrast

In order to understand the differences between the mean ISM onset date in observations, FOR and CTL, Figures 1c and d show the mean seasonal evolution of the TT in the southern and northern boxes used to compute the TTG index. Consistent with previous studies (e.g. Li and Yanai, 1996; and He et al., 2003; Xavier et al., 2007), Figure 1c demonstrates that the establishment and seasonal evolution of ISM are closely related to the variations of the TT fields over the Asian land mass (e.g. the northern box). The mean ISM onset date is mainly controlled by the warming in the Asian region during spring and early summer and not by the evolution of TT over the Indian Ocean, which is rather modest at the seasonal time scale (Figs. 1c and d).

Figures 2a-c show the mean ERAI 2-meter temperature fields just before the ISM onset and the differences with the climatology simulated by FOR and CTL experiments (similar results are obtained with other observed datasets, not shown). The most salient feature is the existence of very warm temperatures (e.g. above 32°C) over Somalia, Saudi Arabia and the Indian subcontinent. Interestingly, both FOR and CTL produce much higher than observed temperatures over the Indian subcontinent and a rather similar land-sea contrast at the surface. A larger warming is also observed over Indochina in CTL. However, in spite of these features, the timing of

307 the ISM onset is largely delayed in CTL compared to observations and FOR. These results suggest
308 that the regional differences in the mid and upper troposphere are the key-factors controlling the
309 ISM onset (and the differences between FOR and CTL), rather than the land-sea thermal contrast
310 near the surface (He et al., 2003; Dai et al., 2013).

311

312 Furthermore, although the change of sign of the TTG is mainly controlled by the seasonal
313 evolution of the TT over the northern box, the seasonal TT warming from the beginning of May to
314 the end of July over this northern box is almost identical in observations, FOR and CTL (Fig. 1c). In
315 contrast, large differences are observed for the same period over the southern box with the
316 observed TT lying between the too warm CTL and too cold FOR estimates (Fig. 1d). The TT time
317 evolution over the southern box is also strikingly different with observations and CTL exhibiting a
318 maximum just before ISM and a minimum during the early part of ISM. This brutal decrease,
319 which is associated with the northward migration of TT maximum (Fig. 1b), occurs later and is
320 weaker in CTL than in the observations. This is consistent with the delayed ISM onset in CTL, since
321 maximum warming in the southern box is usually observed in the pre-monsoon period when the
322 InterTropical Convergence Zone (ITCZ) is located near the equator, and is followed by a slight
323 cooling, when the ITCZ moves northward during the monsoon (Prodhomme et al., 2014).
324 Conversely, the southern box in FOR is characterized by weak maximum values during nearly the
325 whole boreal summer contrary to observations and CTL. This suggests that the good agreement
326 between the mean ISM onset date in observations and FOR may be due to wrong reasons or
327 compensating errors. In this respect, it is worth noting that the shape of the TT seasonal cycle
328 over the southern box is rather similar in observations and CTL, but shifted by one month in CTL.

329

330 In conclusion, the differences of ISM onset in observations, FOR and CTL, are probably controlled
331 by thermodynamic processes over the ocean rather than over the continent. The following
332 subsections examine regional and global factors that may be controlling the modest seasonal
333 warming of TT over the ocean in observations, FOR and CTL, in order to further understand the
334 differences in observed and simulated ISM onset timing.

335

336 **4.2 Daily evolution of regional atmospheric fields and ISM onset**
337 Figure 3 shows latitude-time diagrams of the daily climatologies of precipitation, TT and vertical

338   shear of zonal winds (defined as the difference in zonal winds between 200 minus 850 hPa levels)
339   averaged between 50°E and 90°E in observations, CTL and FOR from March 1st to June 30th. This
340   figure illustrates the tight relationships between the northward migration of precipitation, the
341   reversal of the vertical zonal wind shear and of the TTG associated with the ISM onset in the
342   different datasets. Consistent with the thermal wind relation, the region of strong easterly vertical
343   shear is always located where the meridional TTG is maximum (Webster and Yang, 1992; Dai et
344   al., 2013). Furthermore, this easterly vertical shear of zonal winds seems to be an important factor
345   for sustaining the northward migration of the rain band and, thus, triggering the ISM onset in
346   observations and simulations (Xavier et al., 2007). In turn, through latent heat release in the
347   troposphere, the rainfall plays an important role in the TT evolution over the Indian Ocean. The
348   fact that the TT warming slightly precedes the northward migration of precipitation over the
349   Indian latitudes could suggest a driving role of the TTG over the Indian Ocean for ISM rainfall onset
350   in observations, FOR and CTL (Webster and Yang, 1992; Xavier et al., 2007). Moreover, the parallel
351   evolution of precipitation and TT confirms again the relevance of the TTG index to measure the
352   ISM onset.

353

354   Both FOR and CTL reproduce the northward propagation of precipitation and TT maxima
355   (associated with latent heat release) and the concomitant strengthening of easterly vertical shear
356   of zonal wind (Fig. 3). Nevertheless, Figures 3b, e and h confirm that the transition to the summer
357   monsoon regime is more abrupt in FOR (e.g. it is mainly an instantaneous shift of the rain band)
358   than in observations or CTL. In agreement with Fig. 1d, the transition period between April and
359   May, with maxima of precipitation and TT around the equator, does not exists in this simulation. It
360   also appears that FOR simulates excessive precipitation, TT and easterly vertical shear of zonal
361   wind over northern Indian Ocean and India during ISM (Figs. 3b, e and h). Conversely, CTL
362   reproduces well the progressive transition from winter to monsoon circulations over the Indian
363   Ocean (Figs. 3c, f and i), but the northward migration of precipitation and TT maxima is delayed by
364   nearly one month in CTL, in agreement with the late ISM onset date in this simulation (see Section
365   3 and Fig. 1b). After ISM onset, the two rainfall maxima, both north and south of the equator,
366   which exist in observations and FOR, are merged into an unique broad area, just north of the
367   equator, and important rainfall deficits are noted over India and the south Indian Ocean (Fig. 3c;
368   Prodhomme et al., 2014). Associated with these biases, the TT is too warm around the equatorial

369 Indian Ocean from March to June (Fig. 3f) and this equatorial TT warming seems to play a key role

370 in the delayed ISM onset in CTL. The next subsection will investigate the possible origins of this TT

371 bias in the coupled model.

372

373 **4.3 Tropospheric temperature, convection and tropical SSTs**

374 Figures 2d-f show the observed global distribution of TT, just before the ISM onset, and the

375 differences with FOR and CTL, respectively. Two of the most salient features in observations are

376 the uniformity of the high temperatures over the whole tropics and a maximum over the Indo-

377 Pacific warm pool (Fig. 2d). Both FOR and CTL have difficulties in simulating the exact amplitude

378 of the tropical TT. Despite the cold bias in FOR, consistent with the results of Roeckner et al.

379 (2004), the location of the warmest areas over the western Pacific and eastern Indian oceans is

380 well reproduced, even if the amplitude is too weak (Fig. 2e). In CTL, the situation is just the

381 opposite; the TT is globally warmer in the tropical areas and slightly cooler in the extra-tropical

382 areas compared to observations (Fig. 2f). The pre-monsoon differences between TT over the

383 southern Indian Ocean box in observations, CTL and FOR (Fig. 1d) are not only controlled by local

384 processes in the Indian ocean. Indeed, the tropospheric temperature in this box results of the

385 property of the whole free tropical atmosphere, which is controlled by convection in the whole

386 tropical area.

387

388 Focusing now on the tropical oceans, Figures 2e and f show that the cold tropical bias in FOR is

389 prominent in the tropical Atlantic and Indian oceans while the warm bias in CTL is centered over

390 the tropical Pacific and is symmetrical about the equator. If we look at the boxes used to compute

391 the TTG, both northern and southern boxes are too cold compared to observations in FOR (Fig.

392 2e). However, the cold bias is stronger in the southern than in the northern box, which leads to a

393 TTG, averaged between mid-April and mid-May, stronger than the observed TTG (precisely,

394 +0.34K), which is consistent with the slightly, but still not significant, earlier ISM onset in FOR. In

395 CTL, the bias is opposite, giving a TTG, averaged between mid-April and mid-May, weaker than the

396 observed TTG (precisely, -0.62K), which is consistent with the delayed ISM onset in CTL.

397

398 The main mechanisms driving the tropical TT are well understood. First, the geostrophic

399 adjustment near the equator (with a small Coriolis parameter) implies that "local" TT anomalies

become uniformly distributed over the whole tropical band within a time lag of one or two months (Sobel et al., 2001). On the other hand, the depth of the convection over the Indo-Pacific warm pool explains the TT maxima over this region and is instrumental in the fast redistribution of TT to the other tropical regions because the heating projects onto vertical modes with fast horizontal propagation speeds (Wu et al., 2001). The model precipitation biases are thus expected to be the main source of TT biases seen in Figures 2 and 3. In FOR, the equatorial Indian and western Atlantic oceans are much drier (-4 and -8mm/day, respectively) than observed (Fig. 4e). Less rainfall (-4mm/day) is also simulated in the Pacific equatorial band west of the Date line, compensated by excessive rainfall (6mm/day) at tropical latitudes in both hemispheres. The TT anomalies seem indeed to be closely related to these precipitation biases in FOR (e.g. compare Figs. 2e and 4e). By contrast, CTL simulates excessive precipitation (8mm/day) over the Indo-Pacific warm pool, especially in the western and central equatorial Pacific, compared to both FOR and observations (Figs. 4d and f). This excess of precipitation leads to an important condensational heating, which induces the warm TT bias in the Pacific (Fig. 2f).

Finally, CTL reproduces relatively well the global SST pattern (Figs. 4g-i). Nevertheless, in the equatorial band (except in the well-known cold tongue region; see Masson et al., 2012) and in the coastal upwelling zones (Peru-Chili, California and Benguela), the SST is generally too warm compared to observations (Fig. 4i). These warm biases are collocated with excessive precipitation compared to observations. As an illustration, the spatial correlation between SST biases and rainfall differences between CTL and FOR experiments in the 30°S-30°N tropical band (Figs. 4d and i) has a positive value of 0.54, significant at the 99% confidence level. Thus, SST biases and precipitation anomalies are strongly related in this model, despite of the fact that the anomalous atmospheric response to SST forcing also depends on the background mean state. A cold SST bias is also observed over the Northern Arabian Sea during boreal spring, giving rise to a reduced meridional SST gradient in this area, which may be another important factor affecting both the ISM onset and strength in CTL (Marathayil et al. 2013).

As expected, the TT biases in CTL are primarily sensitive to SST anomalies in areas where the mean SST is high and deep convection frequently occurs (Sobel et al., 2002). During the pre-monsoon period, these regions include the whole equatorial band over the three oceanic basins.

431   Sensitivity experiments have thus been performed in Section 6 in order to discern the relative role
432   of each oceanic basin in the TT warming of the southern box of the TTG (Fig. 1d) and, in the
433   delayed ISM onset simulated in CTL (Figs. 1a, b and Table 1).
434
435   **4.4 Asymmetric mean state: vertical zonal wind shear and humidity**
436   Despite a strong relationship between the ISM onset and the TTG index one month before, the
437   variance of the ISM onset explained by TTG averaged between April 15th and May 15th is only of
438   25% in observations (as estimated by the square of correlation between the two time series): the
439   role of other parameters thus needs to be considered. Many authors have shown that the ISM
440   onset often happens simultaneously with the first episode of the northward propagating ISOs,
441   which occur recurrently during summer and regulate the intraseasonal variability of rainfall over
442   India (Yasunari, 1980; Krishnamurti, 1985; Goswami, 2005b). In this framework, strong (weak)
443   northward propagating ISOs may imply an early (delayed) ISM onset and this may provide an
444   alternative explanation for the differences in onset timing between observations, FOR and CTL
445   experiments.
446
447   Figure 5 displays the lag-composites of 20-80 days filtered daily rainfall anomalies with a Lanczos
448   filter (Duchon, 1979) over a 60 days time window centered on the ISM onset (between 30 days
449   before and 30 days after the ISM onset) in observations, FOR and CTL. This figure illustrates well
450   this possible relationship between the strength of intraseasonal variability and the ISM onset. In
451   observations and FOR, we observe a strong northward propagating ISO at the time of the ISM
452   onset, even though the spatial extent and the propagation speed of these ISOs are different (Figs.
453   5a, b). On the other hand, the amplitude of ISOs is clearly weaker in CTL compared to the amplitude
454   of ISOs in observations and FOR. Interestingly, it seems that the TTG onset slightly precedes the
455   ISO signal in observation. Conversely, in both FOR and CTL, the TTG onset is simultaneous or
456   follows the ISO signal in precipitation.
457
458   Many previous studies have noticed a connection between the northward propagation of the ISOs
459   and the asymmetric mean state with respect to the equator, as manifested in the climatologies of
460   the vertical shear of zonal wind and moisture near the surface (Wang and Xie, 1996; Xie and
461   Wang, 1996; Jiang et al., 2004; Goswami, 2005b; Xiang and Wang, 2013). Therefore, stronger

asymmetry of mean easterly shear and moisture distribution may also be key-factors for explaining the early ISM onset in FOR compared to CTL.

Figure 6 shows the observed and simulated climatologies of the vertical shear of zonal winds and the 850hPa specific humidity in the pre-ISM period, respectively. As anticipated, both fields exhibit a significant equatorial asymmetry in the Indian Ocean and western Pacific, characterized by a northward shift of the easterly shear pattern and more humidity in the northwestern Indian Ocean. This asymmetry may be instrumental for triggering the ISM onset in simulations and observations. The mean easterly vertical shear is weaker in FOR over Asia compare to observations and, even more, compare to CTL (Figs. 6b and c). Both features are clearly related to the meridional gradient of mean TT by the thermal wind relationship (see Section 4.2) and are, thus, dynamically consistent with the weaker TTG in CTL (and also observations) compared to FOR before the ISM onset (Figs. 1b and 3). This may be instrumental for the rapid development of ISM in FOR by enhancing moisture convergence and cyclonic anomalies to the north of the equatorial ITCZ (Jiang et al., 2004).

Several studies have also shown that the speed of the northward propagating ISOs is controlled by the North-South gradient of low-level moisture near the equator (Jiang et al., 2004; Goswami, 2005b). In this respect, another major difference in the Indian Ocean between the two experiments is that the 850hPa moisture tends to be more equatorially trapped in CTL, while the humidity is enhanced between 10°N and 20°N in FOR compared to observations (Figs. 6d-f). This larger (reduced) north-south humidity gradient in the western Indian Ocean, will favor an earlier (delayed) ISM onset in FOR (CTL) by promoting (reducing) positive moisture convergence to the north of the equatorial ITCZ during the pre-ISM period (Jiang et al., 2004). Several observational studies have also shown that moisture build up over the western Arabian Sea significantly leads the ISM onset (Ramesh Kumar et al., 2009). One primary cause for the enhanced moisture near or south of the equator in the western Indian Ocean in CTL compared to FOR and observations (Fig. 6f) appears to be the biased meridional SST gradient in the Arabian Sea in CTL (Fig. 4i) since the specific humidity at the surface (e.g. 1000 hPa) exhibits a similar biased distribution as the one at 850hPa in the western Indian Ocean (not shown). This hypothesis will be confirmed with the help of sensitivity experiments in Section 6.

493

494   The weak moisture gradient and weak easterly shear of zonal winds in CTL may inhibit the

495   northward propagation of the rain band at the intraseasonal time scale (Joseph et al., 2011). While

496   these results are physically consistent with the delayed ISM onset in CTL compared to FOR and

497   observations, the fundamental question of the relative role of local and remote SST biases (in CTL)

498   in shaping these ISM-related spatial distributions of the vertical zonal wind shear and low-level

499   humidity again arises.

500

501   **5. Interannual variability of the ISM onset date**

502

503   This section will investigate the key-factors controlling the ISM onset date interannual variability

504   with the help of a correlation analysis. Many previous studies have suggested that, despite of the

505   SST biases affecting CGCMs, they have better skill than AGCMs as far as the interannual and intra-

506   seasonal variability of ISM is concerned (Wu and Kirtman, 2004; Kumar et al., 2005; Wang et al.,

507   2005; Fu and Wang, 2004; Rajendran and Kitoh, 2006; Fu et al., 2007). Besides identifying ISM

508   onset precursors, another goal of this section is thus to check if this assertion remains valid for

509   the variability of the ISM onset date.

510

511   The correlation maps computed from observations, FOR and CTL experiments have been

512   subjected to a two-tailed t test for statistical significance (von Storch and Zwiers, 2001). Taking

513   into account the level of significance (values above the 90% confidence level will be encircled in

514   the figures) rather than the absolute value of the correlation is important here for interpretation of

515   the results since the lengths of the observed record and the two experiments differ markedly (see

516   Table 1).

517

518   **5.1 ISM onset-surface temperature relationships**

519   We will first discuss the relationship between ISM onset and the surface temperature (SST over

520   ocean and skin temperature over land) and TT fields. The observed SST correlation pattern is

521   reminiscent of El Niño with positive correlations over the central and eastern equatorial Pacific

522   and the classical "horseshoe" pattern of negative correlations extending from the western

523   equatorial Pacific into the subtropics of both hemispheres (Fig. 7a; Annamalai et al., 2005; Terray

and Dominiak, 2005). Thus, as expected, the occurrence of El Niño (La Niña) will tend to delay (promote) the ISM onset (Xavier et al., 2007). Model results also suggest a dominant role of ENSO, particularly the CTL experiment, which reproduces fairly well the observed correlation pattern in the Pacific, even though the area of positive correlation is shifted to the east (Fig. 7c). On the other hand, this ENSO relationship is much less significant in FOR (Fig. 7b). Figure 8a further illustrates that the ISM onset, in observations and both experiments, is significantly associated with Niño3.4 SST during boreal spring, but also with Niño3.4 SST in the previous boreal winter (especially in FOR and observations), in line with many previous studies (Joseph et al., 1994; Annamalai et al., 2005; Park et al., 2010; Boschat et al., 2011; Lau and Nath, 2012). However, the relationship between Niño3.4 SST and ISM onset in CTL is more ambiguous since the correlation is depending on the time evolution, i.e. is maximum at the ISM onset and becomes insignificant 8 months before and after the ISM onset. This suggests a significant impact of ENSO during both its development and decaying phases on the ISM onset date variability in CTL, which is consistent with some observations before the 1980s (e.g. 1972, Joseph et al., 1994; Soman and Slingo, 1997; Boschat et al., 2012), but could also be linked to biases in the representation of ENSO in CTL (Masson et al., 2012; Terray et al., 2012). Despite of this, the shape of the lead-lag correlations with Niño3.4 SSTs is much more realistic in CTL, with correlation increasing steadily to a maximum just before the ISM onset and decreasing afterward as in observations, whereas in FOR the correlation is maximum more than one year ahead of the ISM onset and decreases afterward, month after month (Fig. 8a). This suggests that the physical processes responsible for this ISM onset-ENSO relationship may be different in FOR and CTL, highlighting again the crucial role of air-sea coupling for a proper simulation of the monsoon-ENSO teleconnection (Wu and Kirtman 2004 ; Wang et al. 2005; Krishnan et al., 2010).

We now focus on the potential role of Indian Ocean SST variability. Positive and significant correlation between the ISM onset date and southwest Indian Ocean SSTs exist in observations (Fig. 7a). This is in agreement with previous works suggesting that warm SSTs in this region enhance the local convection and affect significantly the northward migration of the ITCZ and, thus, the timing of ISM (Joseph et al., 1994; Annamalai et al., 2005; Boschat et al., 2011). Positive correlations with central and eastern equatorial Indian Ocean SSTs are also present in observations (Fig. 7a). Francis and Gadgil (2010) have highlighted the possible role of these warm

555   SSTs in suppressing the convection over the Indian continent during the first part of the 2009 ISM

556   through a modulation of the local Hadley cell. FOR also suggests a significant association between

557   ISM onset and SSTs in the central and eastern equatorial Indian Ocean, but the positive

558   correlations with southwest Indian Ocean SSTs are not reproduced (Fig. 7b). Besides, no

559   significant correlations exist between Indian Ocean SSTs and ISM onset in CTL (Fig. 7c).

560

561   In order to further investigate the effect of tropical Indian Ocean SST anomalies, in particular the

562   basin-wide warming that occurs after the mature phase of El Niño (Klein et al., 1999), on the ISM

563   onset date variability, Figure 8b displays the lead-lag correlations between ISM onset date and the

564   monthly Indian Ocean basin mode time series (SST averaged between 40°-110°E and 20°S-20°N;

565   Boschat et al. 2011) in observations and the two experiments. This figure further illustrates that

566   the links between Indian Ocean SSTs and the timing of ISM is much less robust than the one with

567   ENSO. The high positive correlations observed in May-June (e.g. at the ISM onset) in observations

568   and CTL are consistent with the strong dependency of the Indian Ocean SST anomalies during

569   these months on the timing of ISM through latent heat flux and shortwave radiation anomalies

570   (Shukla, 1987; Lau and Nath, 2012). However, FOR fails to reproduce the observed lead-lag

571   relationships between the ISM onset and Indian Ocean SSTs (Fig. 8b). In this context, it should be

572   pointed out that, despite the significant correlations between the ISM onset date time series and

573   SST fields in FOR (Fig. 7b), the correlation between the observed and simulated ISM onset date (in

574   FOR) is only 0.01. This low skill implies that the noise contribution by the atmospheric internal

575   variability is large as far as the ISM onset date variability is concerned (Gouda and Goswami, 2010)

576   and/or that the ocean-atmosphere coupling is essential for a realistic simulation and prediction of

577   the ISM onset date variability (Vitard and Molteni, 2009), as it is for the interannual ISM variability

578   (Wang et al., 2005).

579

580   In other words, AGCM experiments with prescribed SSTs over the Indian Ocean are subject to

581   uncertainties related to the inconsistency between latent heat flux and SST that may lead to

582   spurious atmospheric response, particularly for the timing of the ISM and during boreal summer

583   (Wu and Kirtman, 2004). We suggest that this problem may partly explain the opposite results

584   obtained on the role of Indian Ocean SSTs in the AGCM experiments discussed in Annamalai et al.

585   (2005) and Lau and Nath (2012), for example.

586

587 The ISM onset date is also significantly correlated with SSTs in the Gulf of Benguela in CTL (Fig.

588 7c), but this signal does not exist in observations or FOR. Although some links between ISM and

589 Atlantic variability have been suggested (e.g. Kucharski et al., 2008), this result is probably

590 spurious due to the errors in the mean state over this area in the CTL run (see Section 4).

591

592 Finally, this analysis presents evidence that in observations, FOR and CTL simulations, continental

593 processes occur in conjunction with SSTs in the central Pacific and Indian Ocean to control the ISM

594 onset date. Indeed, there is an inverse relationship between the surface temperature over

595 (northwest) Asia during the pre-ISM period and the ISM onset date (Figs. 7a-c). Besides, these cold

596 temperatures over Pakistan and the Tibetan Plateau have been shown to be significantly

597 correlated with the Niño3.4 SSTs during the previous boreal winter (see Fig. 4d of Boschat et al.,

598 2011). This is consistent with several studies (Yang and Lau, 1998; Shaman and Tziperman, 2005;

599 among others) which suggest that, during the El Niño events, wetter and colder conditions occur

600 over the Asian continent (e.g. more snow and soil moisture over Eurasia), which tend to further

601 weaken the land-sea thermal contrast and lead to a delayed onset and a weakening of the ISM.

602 Another working hypothesis is that these pre-onset temperatures anomalies are the

603 manifestation of land surface processes internal to the monsoon system and not remotely forced

604 by ENSO (Saha et al., 2011; Turner and Slingo, 2010).

605 However, as concerning the Indian Ocean SSTs, the significant negative correlations over land are

606 not located in the same regions in FOR and CTL simulations, suggesting again a significant impact

607 of the coupling in the Indian areas. Interestingly, the temperature correlation pattern over Asia is

608 also more realistic in CTL. This suggests that the SST and land surface processes are to be

609 considered as mutually interactive as far as the ISM onset variability is considered.

610

611 Overall, these findings suggest that the tropical Pacific SST anomalies are the dominant factors in

612 determining the ISM onset date variability in our climate models as well as in observations.

613

614 **5.2 TT, wind shear and low-level moisture relationships**

615 The correlation maps of the ISM onset date with the TT and vertical zonal wind shear during the

616 pre-onset period confirm that the physical processes leading to the ISM onset are very different in

617 FOR and CTL experiments (Figs. 7d-i). A delayed ISM onset in CTL is preceded by positive TT
618 anomalies in the whole tropics and negative easterly shear anomalies of zonal wind over the
619 central Pacific suggesting a weakening of the Pacific Walker circulation. This is physically
620 consistent with the positive correlations with Niño3.4 SSTs (Figs. 7a-c and 8a) as the tropical TT
621 anomalies at the interannual time scale are largely controlled by ENSO (Sobel et al., 2002). All of
622 these associations are also found in the observed TT and wind shear correlation maps, but not in
623 the FOR experiment. By contrast, FOR highlights the existence of cold TT anomalies over the
624 Tibetan Plateau (in agreement with surface temperature anomalies in Figure 7b) and a weakening
625 of the easterly shear of background zonal winds over the North Indian Ocean and Maritime
626 Continent (Fig. 7e) as the main precursors for the delayed ISM onset. Interestingly, these
627 associations are also found in observations, but not in the CTL experiment. A detailed examination
628 from daily data, however, reveals that a delayed ISM onset is usually preceded by a weakening of
629 the easterly wind shear during a period of nearly one month preceding the ISM onset date in all
630 the cases (Fig. 9a). This pre-conditioning is only shifted in time in CTL due to the delayed onset
631 and becomes insignificant if the wind shear is averaged between the 15th April and the 15th May,
632 as in Figure 7i.

633

634 Furthermore, this weakening of the easterly wind shear, associated with a delayed onset, is in
635 phase with a decrease of organized convection over the western Pacific and near the Philippines
636 (120°-150°E and 0°-20°N) in observations and FOR (Fig. 9b; Soman and Slingo, 1997; Joseph et
637 al., 1994, Xiang and Wang, 2013). This link may be physically understood through the propagation
638 of westward Rossby waves from the western Pacific to the Indian Ocean (Xiang and Wang, 2013)
639 or, alternatively, by the fact that the upper level easterly jet moves northwestwards from
640 equatorial to Indian latitudes as ISM develops. This precursory rainfall signal in the western Pacific
641 is of the right sign, but almost insignificant in CTL for a period of one month before the ISM onset
642 (Fig. 9b).

643

644 The high dependence of the ISM onset date variability on the TT variations over land (Fig. 7e),
645 which evolve independently from ENSO in FOR (Fig. 9c), suggests that the ISM onset date
646 variability is largely governed by "internal" monsoon dynamics in FOR, in contrast to observations
647 and CTL. This is in agreement with the fact that FOR has virtually no skill in predicting the ISM

648 onset date (e.g. the absence of correlation between the observed and simulated ISM onset date in
649 FOR, see above), in spite of using the observed SSTs as boundary conditions. This suggests that the
650 forced AGCM may be inappropriate for understanding the physical processes controlling the ISM
651 onset date mean and variability. In order to highlight the key physical processes involved in the
652 ISM onset and delineate the specific role of SSTs in each tropical ocean on the mean ISM onset
653 date, we will thus focus on numerical sensitivity coupled experiments in the next section.
654
655 **6. Sensitivity experiments**
656
657 **6.1 Impact on the mean onset**
658 With the help of the 4 sensitivity experiments described in Section 2.2, we will try to understand
659 how the errors in the representation of the mean state in the different oceanic basins impact the
660 mean ISM onset date in CTL. The focus here is on the role of the mean state SST biases on the time
661 delayed of the mean onset date, not on the variability of the simulated onset date, since it is not
662 straightforward to distinguish in the sensitivity experiments the respective roles of the suppressed
663 variability and the mean SST biases in each corrected region as far as the interannual variability of
664 the onset is concerned (see Section 2.2).
665
666 Figure 10 illustrates again the too early onset in FOR and the delayed onset in CTL (see Section 3).
667 The mean onset date is equivalent in FTPC and CTL. The impact of both Indian and Atlantic Oceans
668 corrections on the onset is more than twice weaker (4 days earlier than in CTL, see Table 2) than
669 the impact of the Pacific Ocean (9 days earlier than in CTL, see Table 2). The CTL's mean onset date
670 is statistically different from all other experiments and observations, except from FTPC's onset
671 date (see Table 2, tested with a two tailed Student t test; Von Storch and Zwiers, 2001). This
672 absence of change of the mean onset date in the FTPC experiment, where the variability of the
673 Pacific is suppressed without correcting the mean state, demonstrates the weak impact of ENSO
674 variability on the delayed mean onset date in CTL. As a result, the misrepresentation of the onset in
675 CTL is not linked to a misrepresentation of ENSO variability (such as the existence of spring ENSO
676 events in CTL; see Masson et al., 2012).
677
678 Figure 11 shows the seasonal cycles of the daily TTG and daily TT averaged in the northern and

679   southern boxes. The TT becomes cooler in both boxes in all sensitivity experiments (except FTPC,
680   Figs. 11b and c). This reflects a global cooling of the free troposphere in the whole tropics, clearly
681   visible on TT mean state (e.g. see Fig. 12b for FTP). In the northern box, this cooling is almost
682   equivalent in FTP, FTA and FTIO (approximately 1°C). In the southern box, the differences
683   between CTL, FTA, FTIO and FTP are stronger, suggesting that the differences between the ISM
684   onset dates in the experiments are largely controlled by the TT variations over the southern box
685   (Fig. 11c).

686

687   In order to explore if these changes of the TTG are associated with different evolutions of the
688   northward propagation of ITCZ over the Indian Ocean, Figure 12 displays latitude-time diagrams of
689   the daily climatology of precipitation averaged between 50°E and 90°E in the different sensitivity
690   experiments from March 1st to June 30th. Both FTIO and FTP simulate an early rainfall ISM onset
691   and an improved evolution of the rain band (Figs. 12b and d). Before the onset, the meridional
692   extent of the ITCZ is larger (as observed) with more significant rainfall to the north of the Equator
693   in these two experiments (e.g. compare with Fig. 3a). Consistent with the sign of the SST
694   corrections, the amplitude of the rainfall signal is also globally reduced in FTIO, especially along the
695   Equator. Surprisingly, the FTP experiment also simulates realistically the existence of two
696   preferred locations of the ITCZ, north and south of the Equator, as in observations and FOR (see
697   Figs. 3a and b). This important feature is missing in CTL, but also in FTIO and FTA. Finally, the
698   correction of the large Atlantic SST biases does not improve significantly the evolution of the ITCZ
699   over the Indian Ocean (Fig. 12c).

700

701   The next sections will investigate the physical mechanisms explaining the larger impact of the
702   Pacific SST correction and the key role of the southern box to explain the differences between the
703   experiments.

704

705   **6.2 Impact of Pacific Ocean mean SST biases on the onset date**
706   The SST corrections applied in FTP have various consequences as shown in Figure 13. Firstly, the
707   precipitation and wind mean states, become extremely close to the mean state of FOR (Fig. 4b, see
708   section 4.3), with an important decrease of precipitation in the equatorial Pacific compared to
709   CTL, associated to an increase of precipitation in the subtropics, which could be summarized as a

northward (southward) migration of the ITCZ (South Pacific Convergence Zone, SPCZ). In the Indian Ocean, precipitation is slightly shifted northwards over the south Arabian Sea, Bay of Bengal and south Asia (Fig. 13c). This indicates an earlier northward migration of the ITCZ, consistent with the earlier ISM onset in this experiment (Fig. 12D and Table 2). These precipitation anomalies in the Indian Ocean are not directly driven by local SST changes, because the cooler Indian Ocean SSTs are supposed to favor an opposite precipitation pattern (Fig. 13a). Therefore, the earlier northward migration of the ITCZ and the associated earlier onset in FTP are linked to the remote impact of SST Pacific corrections.

The earlier onset is, by definition here, linked to the earlier reversal of the TTG. In FTP, the strong decrease of precipitation in the equatorial Pacific (Fig. 13c) leads to a strong decrease of latent heat flux released in the troposphere. This feature explains the large decrease of TT in the Pacific in FTP compared to CTL (Fig. 13b), through the propagation of the classical symmetric Rossby wave (Su et al., 2003). This decrease of TT is also associated with the propagation of a Kelvin wave to the east, which leads to a decreased TT in both equatorial Atlantic and Indian oceans, consistent with previous studies (Su et al., 2003). In the Indian Ocean, the cooling occurs mainly around the equator, which leads to a stronger cooling in the southern box (-1.69°C) than in the northern box (-1.02°C) and, thus, to an increase of TTG. This increase contributes and is symptomatic of an earlier northward migration of ITCZ and an earlier ISM onset.

The vertical wind shear in FTP is largely improved and is more easterly (westerly) than in CTL over the Indian (Pacific) Ocean (Fig. 13e). This more easterly wind shear in FTP, will favor the northward propagation of the ITCZ and the ISOs and thus an advanced ISM onset (Goswami at al., 2010, Xiang and Wang, 2013). We argue that this wind shear improvement in FTP compared to CTL mainly stems from the vastly improved precipitation pattern over the western Pacific in FTP (Fig. 13c).

In FTP, the increased rainfall eastward of the Philippines, probably due to the warmer SST imposed in the sub-equatorial region and the correction of the meridional SST gradient in this area (Fig. 13a), is associated with a vigorous cyclonic cell at low-levels. The Rossby wave response to these precipitation anomalies promotes low-level westerly and high-level easterly wind anomalies over the Indian Ocean (Figs. 13c-e), further enhancing the asymmetric wind shear

during this season (Fig. 6). Incidentally, we note that the precipitation and wind anomaly patterns in the western Pacific in FTP are extremely close to the precipitation anomaly pattern obtained by Xiang and Wang (2013) in their WNP coupled model experiment, when they imposed a warm mean SST in the northwest Pacific near the Philippines in their coupled model (their Fig. 10). This strengthens our argument regarding the key-role of SST correction and associated convection response over the western Pacific, in explaining the changes in ISM onset in FTP.

Figure 13f shows the anomalies of humidity at 850hPa in FTP compared to CTL. The global SST decrease in the Indian Ocean is associated with a global decrease of humidity at low levels, except over the south Arabian Sea, Peninsular India and Bay of Bengal, where precipitation and the associated humidity low-level convergence are consistently increased in FTP. This increase of humidity at 850hPa is not associated with an increase of humidity at 1000hPa, since the humidity near the surface is largely controlled by the "local" cold SST anomalies in FTP (Fig. 13a). This area of increased humidity at 850hPa is collocated with an important area of ascent (Fig. 13d) and we argue that this increase of humidity at 850hPa is due to the increased humidity convergence at low-levels. The increase of humidity in the southeast Arabian Sea and Bay of Bengal is known to be crucial for triggering the ISM onset (Joseph et al. 2003, Ramesh Kumar et al., 2009, Sijikumar and Rajeev, 2012).

To conclude this sub-section, the SST correction in the Pacific Ocean leads to an advanced ISM onset, through the cooperation of 3 consistent physical mechanisms. First, the decrease of precipitation in the equatorial Pacific leads to an important decrease of TT in the whole tropical band, which increases the TTG. Second, the appearance of strong positive precipitation anomalies in the northwestern Pacific leads to a more easterly wind shear in the Indian areas, which favors the northward propagation of ISOs and the ITCZ. Third, this leads to the formation of an area of low-level humidity convergence, precipitation and ascent over the south Arabian Sea and Bay of Bengal, again promoting the ISM onset over India.

6.3 Impact of Atlantic and Indian oceans mean SST biases on the onset date
The ISM onset date occurs 4 days earlier in FTIO and FTA compared to CTL, according to the TTG index. The relatively weak impact of the SST correction in FTIO is surprising, considering the

772 significant Indian Ocean SST biases in CTL (Prodhomme et al., 2014) and the large number of
773 studies which have highlighted the role of Indian Ocean SSTs on the ISM onset (Joseph et al., 1994;
774 Annamalai et al., 2005; Masson et al., 2005; Ramesh Kumar et al., 2009; Boschat et al., 2011;
775 Sijikumar and Rajeev, 2012). Interestingly, the huge SST biases existing in the tropical Atlantic
776 Ocean in CTL (Figs. 4i and 14b) have a similar impact on the ISM onset (based on the TTG) with a
777 delay of 4 days. In this section, we will try to understand the changes occurring in both
778 experiments.
779
780 In FTIO, the SST correction leads to a global decrease of the equatorial precipitation in the Indian
781 Ocean (Fig. 14c), however this decrease is not compensated by a strong increase of precipitation
782 around the southern tip of India and the Bay of Bengal, as it was the case for FTP during the pre-
783 monsoon period (e.g. between the 15th April and the 15th May; Fig. 13c). This last result seems in
784 contradiction with the study of Bollasina and Ming (2013), who have shown a link between the
785 precipitation over the Southwestern equatorial Indian Ocean and precipitation over the North
786 Indian Ocean, through the modulation of the Hadley cell. Nevertheless, there is evidence in FTIO of
787 a response of precipitation to the local SST, but this response occurs only just 15 days before the
788 ISM onset (Fig. 12b). In FTA, there is only a weak impact of SST correction (done in the Atlantic)
789 on precipitation and low-level winds in the Indian Ocean and there is no local signal in
790 precipitation, and low-level winds, which could be consistent with an earlier ISM (Figs. 12c and
791 14d).
792
793 Conversely, in both experiments, there is a strong impact of Indian and Atlantic SST corrections on
794 the Pacific SST mean state and this impact is almost the same in both experiments (Figs. 14c-d).
795 First, a significant weakening of the equatorial SST gradient is observed in the Pacific (Figs. 14a-
796 b). As expected in the framework of the Bjerknes feedback, the equatorial low-level easterlies are
797 weaker and the convection is shifted to the East over the equatorial central Pacific, producing an
798 "El Niño-like" effect in both FTIO and FTA. Thus, we cannot exclude the possibility that any
799 benefits of corrected Indian Ocean or Atlantic Ocean SSTs on the onset are lost by competition and
800 delaying influence from the "El Niño-like" warming pattern in the Pacific in both FTIO and FTA
801 experiments. While many studies have highlighted the impact of both Indian and Atlantic oceans
802 on Pacific variability through a modulation of the Walker circulation (Kug and Kang, 2005;

803   Rodriguez-Fonseca at al., 2009; Frauen and Dommenget, 2012; Keenlyside et al., 2013), there is,
804   however, no signature of a significant modulation of the Walker circulation in both FTIO and FTA,
805   with the exception of the low-level signal in the equatorial central Pacific described above (not
806   shown).
807
808   In order to understand the common changes in the Pacific mean state in FTIO and FTA, Figures
809   14e and f show, respectively, the TT anomalies before the ISM onset in the two experiments. In
810   both cases, the weakened convection over the SST correction region and associated latent heat
811   release lead to a TT cooling symmetric about the equator in the Indian (Atlantic) ocean and a
812   global cooling of the whole equatorial region, due to the classical Rossby and Kelvin responses to a
813   cold SST anomaly along the equator (Su et al., 2003). In both experiments, this "cold" equatorial
814   kelvin wave propagates eastward into the central equatorial Pacific, where it results in persistent
815   anomalous convection and surface westerlies by reducing atmospheric stability, thereby explaining
816   the "Niño-like" anomalies observed in the Pacific. (Figs. 14c-d, see also Terray et al., 2012; Boschat
817   et al., 2013).
818
819   We will now explore the impacts on the vertical shear of zonal wind and the humidity that could
820   explain the slightly earlier onset in FTIO, despite this "El Niño-like" state. Figure 15 shows the
821   anomalies of vertical zonal wind shear and low-level humidity between April 15th and May 15th, in
822   FTIO. In the equatorial Indian Ocean, the easterly vertical shear of zonal wind, which was already
823   too weak in CTL (Figs 6a and c), becomes even weaker in FTIO due to the weakening of the Indian
824   Walker circulation forced by the weaker convection over the eastern Indian Ocean and the El
825   Niño-like state over the Pacific in FTIO (Figs. 14a and c). However, the vertical shear of zonal wind
826   becomes more easterly over the north Indian Ocean and south Asia (Fig. 15a). This feature is
827   mostly due to the appearance of strong easterlies at upper levels over Asia as a response to
828   decreased (increased) rainfall over the eastern equatorial Indian Ocean (China Sea) in FTIO (not
829   shown). This feature suggests a faster transition to the boreal summer circulation in the free
830   troposphere in response to the SST corrections in FTIO.
831
832   The SST correction in FTIO leads to a decrease/increase of the 1000hPa humidity where the
833   imposed SST is colder/warmer than in CTL (not shown). However, there is a strong positive

834 specific humidity anomaly at 850hPa in the southeast Arabian Sea, while the warm SST correction
835 is confined to the North Arabian Sea in FTIO (Figs. 14a and 15b). This maximum of 850 hPa
836 moisture is related to the moisture convergence induced by the low-level equatorial wind
837 divergence in FTIO (Fig. 14c). Many authors have shown that the low-level moisture convergence
838 over this area plays a key role on the ISM onset (Ramesh Kumar et al., 2009; Sijikumar and Rajeev,
839 2012). This feature also promotes an advanced ISM onset in FTIO.

840

841 To conclude, the mean ISM onset date (based on the TTG) is the same in FTIO and FTA. In both
842 experiments, the TTG increases by approximately 0.2K during the pre-monsoon period, which is
843 consistent with the 4 days advanced onset date based on the TTG. However, there is almost no
844 impact of the SST correction on the northward propagation of the ITCZ over the Indian Ocean in
845 FTA. Conversely, an earlier rainfall onset is simulated in FTIO due to more easterly vertical shear
846 of zonal wind over Asia and low-level moisture convergence over the southeast Arabian Sea. In
847 both FTIO and FTA experiments, the El Niño-like mean state induced by the SST correction could
848 contribute to delay the onset, offsetting the benefits of the "local" SST corrections .

849

850 **7. Conclusions**

851

852 Despite the crucial impact of the ISM onset on farming and economy in India, our ability to
853 forecast the onset date is quite low. A limiting factor for the predictability of the onset is the
854 inability of CGCMs to reproduce a realistic mean onset date, with most CGCMs in the CMIP5
855 ensemble simulating a delayed onset (Sperber et al., 2013, Zhang et al., 2012). It thus appears
856 essential to better understand the factors responsible for this delayed onset in CGCMs. Moreover,
857 very few studies have tried to assess the impact of ocean-atmosphere coupling on the ISM onset
858 simulation. We have therefore compared in detail the ISM onset date, its variability and its
859 precursors in observations, and both coupled and atmosphere-only runs. We have also designed
860 several coupled sensitivity experiments, where the SST is nudged to the observed climatology in
861 one oceanic basin at a time, in order to determine the impacts of tropical SST biases elsewhere on
862 the ISM onset.

863

864 We have confirmed the role of three important parameters for triggering the ISM onset (Jiang et

865   al., 2004; Goswami, 2005b; Goswami et al. 2010; Xiang and Wang, 2013):

866   -   The TTG in the Indian Ocean before the onset; an increase of the TTG gradient in the

867   Indian Ocean in the pre-monsoon period favors an earlier reversal and, thus, an earlier onset.

868   However, this parameter alone is not sufficient to explain all the variability of the ISM onset date in

869   coupled and forced simulations or in the sensitivity experiments.

870   -   The vertical shear of zonal wind in the Indian Ocean; a reinforcement of the easterly

871   wind shear favors the northward propagation of the ITCZ, and, thus, promotes an earlier onset.

872   Moreover, an increase of precipitation in the northwestern Pacific also promotes a more easterly

873   wind shear and an early onset (Joseph et al., 1994; Xiang and Wang, 2013).

874   -   The north-south moisture gradient in the northern Indian Ocean; an increase of the

875   moisture just north of the equator favors an earlier onset by promoting northward propagation of

876   ISOs (Jiang et al., 2004; Goswami, 2005b).

877

878   In CTL, the onset estimation, based on the TTG, gives an onset date delayed of 13 days, compared

879   to observations, while in FOR it is 6 days early. In both FOR and CTL, the representation of the 3

880   parameters described above is biased, nevertheless in FOR all of them promote an earlier onset,

881   which explains the 19 days lag between the onset date simulated by FOR and CTL. This difference

882   indicates that the ocean-atmosphere coupling, or SST biases, is responsible for the delayed onset

883   in our CGCM.

884

885   In observations, CTL and FOR, the ISM onset interannual variability is strongly linked to ENSO. As

886   expected, El Niño (La Niña), mostly during its decaying phase, will delay (advance) the ISM onset

887   (Joseph et al., 1994; Xavier et al., 2007; Lau and Nath, 2012). This relationship occurs through two

888   different mechanisms: a warming of the whole equatorial troposphere (e.g. a decrease of the TTG)

889   due to the eastward shift of the convection over the equatorial Pacific during a warm Pacific event

890   (Sobel et al., 2002) and a decrease of precipitation over the northwestern Pacific, associated with a

891   weakening of easterly shear of vertical wind in the Indian Ocean.

892   The forced experiment has no skills to reproduce the observed onset date for a given year and

893   seems to overestimate the role of the interannual variation of the TT in northern Indian Ocean,

894   independently of ENSO, suggesting that the ISM onset date in this experiment is largely governed

895   internal monsoon dynamics. Conversely, it seems that the ENSO-monsoon onset relationship is

better reproduced by CTL. These results demonstrate that the ocean-atmosphere coupling is essential to reproduce the ENSO-ISM onset relationship. Nevertheless, without realistic SSTs in the different tropical regions (and not only in the Indian Ocean) all mechanisms underlying this relationship could not be faithfully reproduced.

To assess more deeply the impact of the misrepresentation of the mean SST on the simulation of the onset date. We performed 3 sensitivity-coupled experiments, where the SST is corrected in each tropical basins.

In the FTP experiment, the correction of SST in the Pacific leads to the strongest improvement of the onset date: 9 days earlier than in CTL. This improvement occurs through a better representation of the 3 parameters described above. Conversely in FTA and FTIO, the correction of the large SST biases in the Atlantic and Indian Ocean, respectively, leads only to a slight improvement of the onset date: 4 days earlier than in CTL. In both experiments, the slightly earlier onset could be explained by the moderate improvement of the TTG due to the correction in either Atlantic or Indian Ocean.

Nevertheless, this absence of impact of the correction in FTIO is surprising since many studies have suggested a key role of Indian Ocean SSTs on the ISM onset (Joseph et al., 1994; Annamalai et al., 2005; Masson et al., 2005; Ramesh Kumar et al., 2009; Boschat et al., 2011; Sijikumar and Rajeev, 2012). Thus, a deeper investigation of the daily seasonal cycle of precipitation shows that, even if the SST correction in the Indian Ocean does not impacts directly onset date, we observe a positive impact of the northward migration of the ITCZ 15 days before the onset. This last improvement in FTIO could be explained by the more easterly vertical shear of zonal wind and by the low level moisture convergence over Arabian Sea.

Moreover in both FTIO and FTA, the SST correction leads to an "El Niño-like" state in the equatorial Pacific, which could also delay the ISM onset, through mechanisms similar to the impact of ENSO on the onset at interannual time scale, offsetting the benefits of the "local" SST corrections on the ISM onset.

Our simulations also suggest an important role of continental processes on the ISM onset date variability (Yang and Lau, 1998). Interestingly, the relationships between land temperatures and the ISM onset are largely overemphasized in the forced simulation and are better simulated in the coupled simulation. This last feature suggests a control of the ocean on the continental surfaces. It

also appears essential now to disentangle the land processes forced by ENSO (Shaman and Tziperman, 2005) from those linked to internal monsoon dynamics over the land (Saha et al., 2011). In this context, Turner and Slingo (2010) have shown that the snow cover may impact the ISM onset independently of ENSO, consistent with the Blanford hypothesis. Nevertheless, Fasullo (2004) have demonstrated a significant weakening of this relationship in the presence of an El Niño event. To better understand the role of continental surfaces, it would be useful to design some sensitivity coupled experiments, similar to those of Turner of Slingo (2010), which modify different continental surface parameters known to impact the ISM onset, as hydrology (Webster, 1983; Rajendran et al., 2002), snow cover (Vernekar et al., 1995; Bamzai and Shukla, 1999; Bamzai and Marx, 2000), vegetation (Yamashima et al., 2011), soil moisture and surface temperature, in the presence or absence of ENSO. These types of experiments could provide useful answers on the respective role of ocean and continental surfaces for the ISM onset and the monsoon.

In this study, we have proposed some oceanic mechanisms to explain the delayed ISM onset in a coupled model. An important issue is now to determine whether the Pacific SST biases may also play a key role in explaining the delayed ISM onset in the CMIP5 database through the variations of the TTG, easterly wind shear and moisture gradient, as in the SINTEX CGCM. Similar comparisons between CMIP5 coupled models and their atmosphere-only counterparts could also provide us with some additional answers or clues as to explain the misrepresentation of the ISM onset and the importance of the coupling. Such multi-model comparison analyses appear now essential to study the evolution of the ISM onset in a climate change context, since many recent studies have shown an impact of SST increasing trend or multidecadal variability in the tropical Pacific on the ISM onset (Goswami et al., 2010; Xiang and Wang, 2013).

References

958 Abe M, Hori M, Yasunari T, Kitoh A (2013) Effects of the Tibetan Plateau on the onset of the
959 summer monsoon in South Asia: The role of the air-sea interaction. Journal of Geophysical
960 Research, 118, 1760-1776. doi:10.1002/jgrd.50210

961

962 Ananthakrishnan R, Soman MK (1988) The onset of the southwest monsoon over Kerala: 1901-
963 1980. Journal of Climatology 8: 283–296. doi:10.1002/joc.3370080305.

964

965 Annamalai H, Liu P, Xie S-P (2005) Southwest Indian Ocean SST variability: Its local effect and
966 remote influence on Asian Monsoons. Journal of Climate, 18, 4150–4167

967

968 Bamzai A, Shukla J (1999) Relation between Eurasian snow cover, snow depth, and the Indian
969 summer monsoon: An observational study. Journal of Climate 3117–3132. Doi: 10.1175/1520-
970 0442(1999)012<3117:RBESCS>2.0.CO;2

971

972 Bamzai A, Marx L (2000) COLA AGCM simulation of the effect of anomalous spring snow over
973 Eurasia on the Indian summer monsoon. Quarterly Journal of the Royal Meteorological Society
974 2575–2584. doi: 10.1002/qj.49712656811

975

976 Bollasina M and Ming Y (2013) The general circulation model precipitation bias over the
977 southwestern equatorial Indian Ocean and its implications for simulating the South Asian
978 monsoon. Climate Dynamics, 40(3-4), DOI:10.1007/s00382-012-1347-7

979

980 Boschat G, Terray P, Masson S (2011) Interannual relationships between Indian Summer Monsoon
981 and Indo-Pacific coupled modes of variability during recent decades. Climate Dynamics 37: 1019–
982 1043. doi:10.1007/s00382-010-0887-y

983

984 Boschat G, Terray P, Masson S (2012) Robustness of SST teleconnections and precursory patterns
985 associated with the Indian summer monsoon. Climate Dynamics 38: 2143–2165.
986 doi:10.1007/s00382-011-1100-7

987

988 Boschat, G., P. Terray, and S. Masson (2013), Extratropical forcing of ENSO, Geophys. Res. Lett. , 40

,1–7, doi:10.1002/grl.50229.

Cherchi A, Navarra A (2003) Reproducibility and predictability of the Asian summer monsoon in the ECHAM4-GCM. Climate Dynamics. Springer 20: 365–379. doi:10.1007/s00382-002-0280-6

Dai et al. (2013) The relative roles of upper and lower tropospheric thermal contrasts and tropical influences in driving Asian summer monsoons. Journal of geophysical research: Atmospheres, Vol. 118, 7024–7045, doi:10.1002/jgrd.50565

Dee DP, and Coauthors (2011): The ERA-Interim reanalysis: Configuration and performance of the data assimilation system. Quarterly Journal of Royal Meteorological Society, 137, 553–597. doi: 10.1002/qj.828

Duchon CE (1979) Lanczos filtering in one and two dimensions. Journal of Applied Meteorology **18:** 1016–1022

Fasullo J, Webster P (2003) A hydrological definition of Indian monsoon onset and withdrawal. Journal of Climate, 16, 3200–3211

Fasullo J (2004) A stratified diagnosis of the Indian monsoon-Eurasian snow cover relationship. Journal of Climate, 17(5):1110–1122

Flatau M, Flatau P, Rudnick D (2001) The dynamics of double monsoon onsets. Journal of Climate 14: 4130–4146. doi:10.1175/1520-0442(2001)014<4130:TDODMO>2.0.CO;2

Flohn H (1957): Large-scale aspects of the "summer monsoon" in south and east Asia. Journal of Meteorological Society of Japan, 35, 180–186.

Francis PA, Gadgil S (2010): Towards understanding the unusual Indian monsoon in 2009. Journal of Earth System Science, 119, 397–415.

1018

1019 Frauen, C., and D. Dommenget (2012), Influences of the tropical Indian and Atlantic Oceans on the

1020 predictability of ENSO, Geophys. Res. Lett., 39(2), L02706, doi:10.1029/2011GL050520.

1021

1022 Fu, X., B. Wang, T. Li, and J. McCreary (2003) Coupling between Northward-Propagating,

1023 Intraseasonal Oscillations and Sea Surface Temperature in the Indian Ocean. *Journal of*

1024 *Atmospheric Science.,* 60, 15, 1733-1753.

1025

1026 Fu, X., and B. Wang (2004) The boreal summer intraseasonal oscillations simulated in a hybrid

1027 coupled atmosphere-ocean model. *Monthly Weather Review* 132, 2628-2649.

1028

1029 Fu, X., B. Wang, D. E. Waliser, and L. Tao (2007) Impact of atmosphere–ocean coupling on the

1030 predictability of monsoon intraseasonal oscillations. *Journal of Atmospheric Science,* 64, 157–174.

1031

1032 Goswami BN (2005a) South Asian Summer Monsoon: An overview: in The Global Monsoon

1033 System: Research and Forecast. Chang C-P, Wang B, Gabriel Lau N-C (eds). Chapter 5, pp 47, WMO

1034 TD No. 1266, WMO, Geneva.

1035

1036 Goswami BN (2005b) South Asian monsoon. In Intraseasonal Variability in the Atmosphere-Ocean

1037 Climate System, LauWK-M, Waliser DE (eds). Springer-Praxis publication: Berlin, 19–62.

1038

1039 Goswami B, Xavier P (2005) ENSO control on the south Asian monsoon through the length of the

1040 rainy season. Geophysical Research Letters 32: L18717. doi:10.1029/2005GL023216

1041

1042 Goswami B, Kulkarni J, Mujumdar V, Chattopadhyay R (2010) On factors responsible for recent

1043 secular trend in the onset phase of monsoon intraseasonal oscillations. International Journal of

1044 Climatology 30: 2240–2246. doi:10.1002/joc.2041

1045

1046 Goswami P, Gouda KC (2010) Evaluation of a Dynamical Basis for Advance Forecasting of the Date

1047   of Onset of Monsoon Rainfall over India. Monthly Weather Review 138: 3120–3141.
1048   doi:10.1175/2010MWR2978.1

1049

1050   Guilyardi, E., P. Delecluse, S. Gualdi, and A. Navarra (2003), Mechanisms for ENSO phase change in
1051   a coupled GCM, Journal of Climate. 16,1141–1158.

1052

1053

1054   He H, Sui C-H, Jian M, Wen Z, Lan G (2003) The Evolution of Tropospheric Temperature Field and
1055   its Relationship with the Onset of Asian Summer Monsoon. Journal of the Meteorological Society of
1056   Japan 81: 1201–1223. doi:10.2151/jmsj.81.1201

1057

1058   Huffman GJ, Adler RF, Arkin P, Chang A, Ferraro R, Gruber A, Janowiak J, McNab A, Rudolf B,
1059   Schneider U (1997) The global precipitation climatology project (GPCP) combined precipitation
1060   dataset. BAMS 78:5–20

1061

1062   Jiang XN, Li T, Wang B (2004) Structures and mechanisms of the northward propagating boreal
1063   summer intraseasonal oscillation. Journal of Climate 17, 1022–1039

1064

1065   Joseph P, Eischeid J, Pyle R (1994) Interannual variability of the onset on the Indian summer
1066   monsoon and its association with atmospheric features, El Niño, and sea surface temperature
1067   anomalies. Journal of Climate, **7**, 81–105.

1068

1069   Joseph P, Sooraj K, Rajan C (2006) The summer monsoon onset process over South Asia and an
1070   objective method for the date of monsoon onset over Kerala. International Journal of Climatology
1071   1893: 1871–1893. doi:10.1002/joc

1072

1073   Joseph S, Sahai A, Goswami B, Terray P, Masson S, Luo J-J (2011) Possible role of warm SST bias in
1074   the simulation of boreal summer monsoon in SINTEX-F2 coupled model. Climate Dynamics.
1075   doi:10.1007/s00382-011-1264-1

1076

1077   Klein, SA., Soden BJ, Lau NC, 1999: Remote Sea Surface Temperature Variations during ENSO:

Evidence for a Tropical Atmospheric Bridge. *Journal of Climate*, **12**, 917–932.

Klingaman NP, Woolnough SJ, Weller H, Slingo JM (2011) The Impact of Finer-Resolution Air–Sea Coupling on the Intraseasonal Oscillation of the Indian Monsoon. Journal of Climate 24: 2451–2468. doi:10.1175/2010JCLI3868.1

Kripalani RH, Oh JH, Kulkarni a., Sabade SS, Chaudhari HS (2007) South Asian summer monsoon precipitation variability: Coupled climate model simulations and projections under IPCC AR4. Theoretical and Applied Climatology 90: 133–159. doi:10.1007/s00704-006-0282-0

Krishnamurti T. 1985. Summer monsoon experiment – A review. Monthly Weather Review 113: 1590–1626.

Krishnan R, Sundaram S, Swapna P, Kumar V, Ayantika DC, Mujumdar M (2010) The crucial role of ocean-atmosphere coupling on the Indian monsoon anomalous response during dipole events. Climate Dynamics doi:10.1007/s00382-010-0830-2

Kucharski F, Bracco a., Yoo JH, Molteni F (2008) Atlantic forced component of the Indian monsoon interannual variability. Geophysical Research Letters 35: L04706. doi:10.1029/2007GL033037

Kug, J. S., S. I. An, F. F. Jin, and I. S. Kang (2005), Preconditions for El Niño and La Niña onsets and their relation to the Indian ocean, Geophys. Res. Lett. , 32 (L05), 706, doi:10.1029/2004GL021674

Kummerow C, and Coauthors (2001) The Evolution of the Goddard Profiling Algorithm (GPROF) for Rainfall Estimation from Passive Microwave Sensors. Journal of Applied Meteorology, 40, 1801–1820

Lau N-C, Nath MJ (2012) A Model Study of the Air–Sea Interaction Associated with the Climatological Aspects and Interannual Variability of the South Asian Summer Monsoon Development. Journal of Climate 25: 839–857. doi:10.1175/JCLI-D-11-00035.1

1109 Lee E, Chase T, Rajagopalan B, Barry RG, Biggse TW, Lawrence PJ (2009) Effects of irrigation and
1110 vegetation activity on early Indian summer monsoon variability. International Journal of
1111 Climatology 581: 573–581. doi:10.1002/joc

1113 Lee et al. (2013) Real-time multivariate indices for the boreal summer intraseasonal oscillation
1114 over the Asian summer monsoon region. Climate Dynamics, 40:493–509

1116 Luo J-J, Masson S, Behera S K, Delecluse P, Gualdi S, Navarra A, Yamagata T (2003) South Pacific
1117 origin of the decadal ENSO-like variation as simulated by a coupled GCM. Geophysical Research
1118 Letters, 30, 2250, doi:10.1029/ 2003GL018649

1120 Luo J-J, Masson S, Roeckner E, Madec G, Yamagata T (2005) Reducing Climatology Bias in an
1121 Ocean–Atmosphere CGCM with Improved Coupling Physics. Journal of Climate 18: 2344–2360.
1122 doi:10.1175/JCLI3404.1

1124 Madec G (2008) NEMO ocean engine. Note du Pole de modelisation, Institut Pierre-Simon Laplace
1125 (IPSL) No 27. ISSN No 1288– 1619

1127 Masson S, Luo J-J, Madec G et al. (2005) Impact of barrier layer on winter-spring variability of the
1128 southeastern Arabian Sea. Geophysical Research Letters 32: L07703. doi:10.1029/2004GL021980

1130 Masson S, Terray P, Madec G, Luo J-J, Yamagata T, Takahashi K (2012) Impact of intra-daily SST
1131 variability on ENSO characteristics in a coupled model. Climate Dynamics. doi:10.1007/s00382-
1132 011-1247-2

1133 Marathayil D, Turner A G, Shaffrey L C, R Clevine RC (2013) Systematic winter sea-surface
1134 temperature biases in the northern Arabian Sea in HiGEM and the CMIP3 models, Environmental
1135 Research Letter 8 014028. doi:10.1088/1748-9326/8/1/014028

1137 Minoura D, Kawamura R, Matsuura T (2003) A mechanism of the onset of the South Asian

1138 Summer Monsoon. Journal of the meteorological Society of Japan, 81, 563-580.

1139

1140 Nordeng TE (1994) Extended versions of the convective parametrization scheme at ECMWF and
1141 their impact on the mean and transient activity of the model in the Tropics. ECMWF Research
1142 Department, Techn Mem 206, October 1994, European Center for Medium Range Weather
1143 Forecasts, Reading, UK, pp

1144

1145 Pai DS, Nair RM (2009) Summer monsoon onset over Kerala: New definition and prediction.
1146 Journal of Earth System Science 118: 123–135. doi:10.1007/s12040-009-0020-y

1147

1148 Prodhomme C, Terray P, Masson S, Izumo T, Tozuka T, Yamagata T (2014) Impacts of Indian Ocean
1149 SST biases on the Indian Monsoon: as simulated in a global coupled model. Climate Dynamics, 42,
1150 271-290. doi:10.1007/s00382-013-1671-6

1151

1152 Ramesh Kumar MR, Sankar S, Reason C (2009) An investigation into the conditions leading to
1153 monsoon onset over Kerala. Theoretical and Applied Climatology 95: 69–82. doi:10.1007/s00704-
1154 008-0376-y

1155

1156 Rajagopalan B and Molnar P (2013) Signatures of Tibetan Plateau heating on Indian summer
1157 monsoon   rainfall   variability.   Journal   of   geophysical   research,   Vol.   118,   1–9,
1158 doi:10.1002/jgrd.50124

1159 Rajendran K, Nanjundiah RS, Srinivasan J (2002) The impact of surface hydrology on the
1160 simulation   of   tropical   intraseasonal   oscillation   in   NCAR   (CCM2)   atmospheric   GCM.   J.
1161 Meteorological Society of Japan, 80, 1357-1381.

1162

1163 Rajendran K, Kitoh A. (2006) Modulation of tropical intraseasonal oscillations by ocean–
1164 atmosphere coupling. Journal of Climate 19: 366–391. doi: 10.1175/JCLI3638.1

1165

1166 Ratna SB, Sikka DR, Dalvi M, Venkata Ratnam J (2011) Dynamical simulation of Indian summer
1167 monsoon circulation, rainfall and its interannual variability using a high resolution atmospheric

general circulation model. International Journal of Climatology 31: 1927–1942. doi:10.1002/joc.2202

Reynolds RW, Smith TM, Liu C, Chelton DB, Casey KS, Schlax MG (2007) Daily High-Resolution-Blended Analyses for Sea Surface Temperature. Journal of Climate 20: 5473–5496. doi:10.1175/2007JCLI1824.1

Rodriguez-Fonseca,B.,I.Polo, J. Garcia-Serrano,T. Losada, E. Mohino, C. R. Mechoso, and F. Kucharski (2009), Are Atlantic Niños enhancing Pacific ENSO events in recent decades?, Geophys. Res. Lett.,36(20), L20705,doi:10.1029/2009GL040048.

Roeckner E, Baüml G, Bonaventura L, Brokopf R, Esch M, Girogetta M, Hagemann S, Kirchner I, Kornblueh L, Manzini E, Rhodin A, Schlese U, Schulzweida U, Tompkins A (2003) The atmospheric general circulation model ECHAM 5, Part I, MPI Report 349:137p. Max-Planck-Institut für Meteorologie, Hamburg

Roeckner E, Brokopf R, Esch M, Giorgetta M, Hagemann S, Kornblueh L, Manzini E, Schlese U, Schulzweida U (2004) The atmospheric general circulation model ECHAM5 Part II: sensitivity of simulated climate to horizontal and vertical resolution. Max-Planck-Institute for Meteorology, MPI-Report 354, Hamburg

Saha SK, Halder S, Kumar KK, Goswami BN (2010) Pre-onset land surface processes and "internal" interannual variabilities of the Indian summer monsoon. Climate Dynamics 36: 2077–2089. doi:10.1007/s00382-010-0886-z

Sankar S, Kumar MRR, Reason C (2010) On the relative roles of El Niño and Indian Ocean Dipole events on the Monsoon Onset over Kerala. Theoretical and Applied Climatology 103: 359–374. doi:10.1007/s00704-010-0306-7

Sato T, Kimura F (2007) How Does the Tibetan Plateau Affect the Transition of Indian Monsoon Rainfall? Monthly Weather Review 135: 2006–2015. doi:10.1175/MWR3386.1

1199

1200   Shaman J, Tziperman E (2005) The effect of ENSO on Tibetan Plateau snow depth: a stationary

1201   wave teleconnection mechanism and implications for the South Asian monsoons. Journal of

1202   Climate. 18:2067–2079. Doi: 10.1175/JCLI3391.1

1203

1204   Shukla J (1987) Interannual variability of monsoons. In Monsoons, edited by JS Fein and PL

1205   Stephens, 399-464, John Wiley and sons.

1206

1207   Sijikumar S, Rajeev K (2012) Role of the Arabian Sea Warm Pool on the Precipitation

1208   Characteristics during the Monsoon Onset Period. Journal of Climate 25: 1890–1899.

1209   doi:10.1175/JCLI-D-11-00286.1

1210

1211   Sobel AH, Nilsson J, Polvani LM (2001) The weak temperature gradient approximation and

1212   balanced tropical moisture waves. J. Atmos. Sci., 58, 3650–3665.

1213

1214   Sobel A, Held I, Bretherton C (2002) The ENSO signal in tropical tropospheric temperature.

1215   Journal of Climate, 15, 2702–2706.

1216

1217   Soman MK, Slingo J (1997) Sensitivity of the Asian summer monsoon to aspects of sea surface

1218   temperature anomalies in the tropical pacific ocean. Quarterly Journal of the Royal Meteorological

1219   Society 309–336

1220

1221   Sperber KR, Annamalai H, Kang IS, Kitoh A, Moise A, **Turner A**, Wang B, Zhou T (2013) The Asian

1222   Summer Monsoon : An intercomparison of CMIP5 vs. CMIP3 simulations of the late 20th Century.

1223   Climate Dynamics, 41, 2711-2744, doi: 10.1007/s00382-012-1607-6.

1224

1225   Su H, Neelin JD, Meyerson JE (2003) Sensitivity of tropical tropospheric temperature to sea surface

1226   temperature forcing. Journal of Climate, 16, 1283-1301

1227

1228   Taniguchi K, Koike T (2006) Comparison of definitions of Indian summer monsoon onset: better

1229   representation of rapid transitions of atmospheric conditions. Geophys Res Lett 33:L02709. doi:

1230   10.1029/2005GL024526

1231

1232   Terray, P. (2011), Southern Hemisphere extra-tropical forcing: a new paradigm for El Niño-

1233   Southern Oscillation, Clim. Dyn. ,36 (11), 2171–2199, doi:10.1007/s00382-010-0825-z

1234

1235   Terray P, Dominiak S (2005) Indian Ocean sea surface temperature and El Niño-Southern

1236   Oscillation: A new perspective. Journal of climate 1351–1368. doi: 10.1175/JCLI3338.1

1237

1238   Terray P, Kamala K, Masson S, Madec G, Sahai A K, Luo J-J, Yamagata T, (2012) The role of the intra-

1239   daily SST variability in the Indian monsoon variability and monsoon-ENSO–IOD relationships in a

1240   global coupled model. Climate Dynamics, 39, 729-754. doi:10.1007/s00382-011-1240-9

1241

1242   Tiedtke M (1989) A Comprehensive Mass Flux Scheme for Cumulus Parameterization in Large-

1243   Scale Models. Monthly Weather Review 117: 1779–1800. doi:10.1175/1520-

1244   0493(1989)117<1779:ACMFSF>2.0.CO;2

1245

1246   Timmermann R, Goosse H, Madec G, Fichefet T, Ethe C, Duliere V (2005) On the representation of

1247   high latitude processes in the ORCA-LIM global coupled sea ice-ocean model. Ocean Modelling, 8(1–

1248   2):175–201

1249

1250   Turner a. G, Slingo JM (2011) Using idealized snow forcing to test teleconnections with the Indian

1251   summer monsoon in the Hadley Centre GCM. Climate Dynamics 36: 1717–1735.

1252   doi:10.1007/s00382-010-0805-3

1253

1254   Valcke S (2006), OASIS3 user guide (prism_2-5), PRISM support initiative 3, 68 pp

1255

1256   Vernekar A, Zhou J, Shukla J (1995) The Effect of Eurasian Snow Cover on the Indian Monsoon.

1257   Journal of Climate, 8, 248-266. doi: 10.1175/1520-442(1995)008<0248:TEOESC>2.0.CO;2

1258

1259   Vitart F, Molteni F (2009) Dynamical Extended-Range Prediction of Early Monsoon Rainfall over

India. Monthly Weather Review 137: 1480–1492. doi: 10.1175/2008MWR2761.1

Von Storch H, Zwiers FW (2001) Statistical analysis in climate research. Cambridge University Press, 484 pp.

Wang B (2006) The Asian monsoon. Springer/Praxis Publishing, New York, 787 pp.

Wang B, Kang I, Lee J (2004) Ensemble Simulations of Asian-Australian Monsoon Variability by 11 AGCMs. Journal of Climate, 17, 803–818

Wang, B., Q. Ding, X. Fu, I.-S. Kang, K. Jin, J. Shukla, and F. Doblas-Reyes, 2005: Fundamental challenges in simulation and prediction of summer monsoon rainfall, *Geophysical Research Letters.*, 32, L15711,doi: 10.1029/2005GL022734 12.

Wang B ,Ding Q, Joseph V (2009) Objective definition of the Indian summer Monsoon onset using large scale winds. *Journal of Climate*, 22, 3303–3316.

Wang B, Xie X (1996) Low-Frequency Equatorial Waves in Vertically Sheared Zonal Flow. Part I: Stable Waves. Journal of the Atmospheric Sciences, 53, 449–467. doi:10.1175/1520-0469(1996)053<0449:LFEWIV>2.0.CO;2

Wang B, LinHo (2002) Rainy Season of the Asian-Pacific Summer Monsoon. Journal of Climate, 15, 386–398. doi:10.1175/1520-0442(2002)015<0386:RSOTAP>2.0.CO;2

Webster P (1983) Mechanisms of monsoon low-frequency variability: Surface hydrological effects. Journal of the atmospheric Sciences, 40, 2110-2124 doi:10.1175/1520-0469(1983)040<2110:MOMLFV>2.0.CO;2

Webster PJ, Magana VO, Palmer TN, Shukla J, Tomas RA, Yanai M, Yasunari T (1998) Monsoons: Processes, predictabililty, and the Prospects for prediction. J. Geophys. Res., 103, C7, 14,451-14,510. doi:10.1029/97JC02719

1291

1292 Woolnough SJ, Vitart F, Balmaseda MA (2007) The role of the ocean in the Madden–Julian

1293 oscillation: implications for MJO prediction. Q J R Meteorol Soc 133:117–128

1294

1295 Wu Z, Sarachik ES, Battisti DS (2001) Thermally driven tropical circulations under Raleigh friction

1296 and Newtonian cooling/ analytic solutions. Journal of Atmospheric sciences, 58, 724-741.

1297

1298 Wu R, Kirtman B (2004) Understanding the impacts of the Indian Ocean on ENSO variability in a

1299 coupled   GCM.   Journal   of   climate   4019–4031.   doi:10.1175/1520-

1300 0442(2004)017<4019:UTIOTI>2.0.CO;2

1301

1302 Xavier PPK, Marzin C, Goswami B (2007) An objective definition of the Indian summer monsoon

1303 season and a new perspective on the ENSO – monsoon relationship. Quarterly Journal of the Royal

1304 Meteorological Society 764: 749–764. doi:10.1002/qj

1305

1306 Xiang B, Wang B (2013) Mechanisms for the Advanced Asian Summer Monsoon Onset since the

1307 Mid-to-Late 1990s. Journal of Climate 26: 1993–2009. doi:10.1175/JCLI-D-12-00445.1

1308

1309 Xie, X. and B. Wang, 1996: Low-frequency equatorial waves in vertically sheared zonal flows. Part

1310 II: unstable waves. *Journal of Atmospheric Science*, 53, 3589-3605.

1311

1312 Yamashima R, Takata K, Matsumoto J, Yasunari T (2011) Numerical Study of the Impacts of Land

1313 Use/Cover Changes Between 1700 and 1850 on the Seasonal Hydroclimate in Monsoon Asia.

1314 Journal of the Meteorological Society of Japan 89A: 291–298. doi:10.2151/jmsj.2011-A19.

1315

1316 Yanai M, Li C, Song Z (1992) Seasonal heating of the Tibetan plateau and its effects on the evolution

1317 of the Asian summer monsoon. Journal of the Meteorological Society of Japan, 70, 319-351.

1318

1319 Yanai M, Li C (1994) Mechanism of heating and the boundary layer over the Tibetan Plateau.

1320 Monthly Weather Review 122: 305–323.

1321

1322 Yang S, Lau KM (1998) Influences of sea surface temperature and ground wetness on Asian
1323 summer monsoon. Journal of Climate 11: 3230– 3246.

1324

1325 Yasunari T (1980) A Quasi-Stationary Appearance of 30 to 40 Day Period in the Cloudiness
1326 Fluctuations during the Summer Monsoon over India. J. Meteor. Soc. Japan, 58, 3, 225-229.

1327

1328 Zhang H, Liang P, Moise a., Hanson L (2012) Diagnosing potential changes in Asian summer
1329 monsoon onset and duration in IPCC AR4 model simulations using moisture and wind indices.
1330 Climate Dynamics 39: 2465–2486. doi:10.1007/s00382-012-1289-0

1331

1332

1333 **Table 1**: Summary of all experiments.

1334

1335

1336 **Table 2:** Mean onset date. Mean values marked with an * are 90% statistically different of the
1337 CTL's mean onset date (tested with a two-tailed Student t test).

1338

1339

1340

1341

1342

1343

1344

1345

1346

1347

1348 **Table 1**

Name	CTL	FOR	FTA	FTPC	FTP	FTIO
Type	CGCM	AGCM	CGCM	CGCM	CGCM	CGCM
Correction area			Atlantic Ocean 100°W-20°E	Pacific Ocean 100°E-70°W	Pacific Ocean 100°E-70°W	Indian Ocean 30°E-120°E

			25°S-25°N	25°S-25°N	25°S-25°N	25°S-30°N
Smoothing area			30°S-25°S 25°N-30°N	30°S-25°S 25°N-30°N	30°S-25°S 25°N-30°N	30°S-25°S
SST data		AVHRR	AVHRR	CTL	AVHRR	AVHRR
Time duration (Year)	110	29	50	30	50	50

1349

1350

1351

1352

1353

1354

1355 **Table 2**

	ERAI	FOR	CTL	FTA	FTIO	FTP	FTPC
Mean onset date (in Julian days)	148,7*	142,8*	161,6	158,2*	157,6*	152,1*	163.8

1356

1357

1358

1359

1360 **Figure legends**

1361

1362 <u>**Figure 1**</u>:

1363   a)   Annual cycle of daily continental precipitation (in mm/day) averaged over the
1364   Indian subcontinent (70°-95°E, 5°-20°N).

1365   b)   Annual cycle of daily TTG (Tropospheric Temperature Gradient, in K) defined as the
1366   difference of the TT (Tropospheric Temperature, temperature averaged between 600 and
1367   200 hPa) averaged in a northern box (40°-100°E; 5°- 35°N) and a southern box (40°-
1368   100°E; 15°S-5°N).

1369   c)   Annual cycle of the daily TT (in K) averaged in the northern box (40°-100°E; 5°-

1370 35°N).

1371 d) Annual cycle of the daily TT (in K) averaged in the southern box (40°-100°E; 15°S-

1372 5°N).

1373 Observations are shown in black (TT is derived from ERA interim, precipitations are derived from

1374 TRMM). Coupled and forced experiments are shown in red and light blue, respectively.

1375

1376 **Figure 2**:

1377 a) Climatology of the ERAI 2-meter temperature calculated between April 15th April and

1378 May 15th for observations (shaded, in °C, contour interval: 1°C).

1379 b) Difference between FOR and ERAI climatologies of 2m temperature (shaded, in °C,

1380 contour interval: 0.4°C) calculated between April 15th and May 15th.

1381 c) Same as b), but for CTL minus ERAI.

1382 d) Same as a) but for the climatology of TT (Tropospheric Temperature, temperature

1383 averaged between 600 and 200 hPa, in K, contour interval: 1K). The TT is estimated from

1384 ERA interim.

1385 e) Difference between FOR and ERAI climatologies of TT (shaded, in K, contour interval:

1386 0.25 K) calculated between April 15th and May 15th.

1387 f) Same as e) but for CTL minus ERAI.

1388 For figures a, b and c, Orography is shown in contours (contour min=1000 m, contour

1389 max=8000 m, contour interval=1000 m).

1390 For figures e and f, the black boxes show the northern (40°-100°E; 5°- 35°N) and the

1391 southern (40°-100°E; 15°S-5°N) boxes used to compute the TTG.

1392

1393 **Figure 3**:

1394 a) Time-latitude diagram of daily climatology of TRMM precipitation (in mm/day, contour

1395 interval: 1.5mm/day) averaged between 50°-90°E, between March 1st and June 30th.

1396 b) Same as a) but for FOR.

1397 c) Same as a) but for CTL.

1398 d) Same as a) but for ERAI TT (Tropospheric Temperature, temperature averaged

1399 between 600 and 200 hPa, in K, contour interval: 0.5K).

1400 e) Same as d) but for FOR.

1401   f) Same as d) but for CTL.

1402   g) Same as a) but for vertical shear of zonal wind (difference between zonal wind,

1403   estimated from ERAI, at 200 and 850 hPa, units: m/s, contour interval: 5m/s).

1404   h) Same as g) but for FOR.

1405   i) Same as g) but for CTL.

1406

1407

1408   **Figure 4**:

1409   a) Climatology of precipitation (shaded, unit in mm/day, contour interval: 1mm/day) and

1410   850hPa winds (arrows, unit in m/s) calculated between April 15th and May 15th for

1411   observations. The precipitation and low-level winds climatologies are estimated from

1412   TRMM and ERAI, respectively.

1413   b) Same as a), but for FOR.

1414   c) Same as a), but for CTL.

1415   d) Difference between CTL and FOR climatologies calculated between April 15th and May

1416   15th for precipitation (shaded, unit in mm/day, contour interval: 1mm/day) and 850 hPa

1417   winds (arrows, unit in m/s).

1418   e) Same as d), but for the difference between FOR and observations.

1419   f) Same as d), but for the difference between CTL and observations.

1420   g) Climatology of observed SST (in °C, contour interval: 0.5°C) calculated between April

1421   15th and May 15th for observations, estimated from AVHRR.

1422   h) Same as g), but for CTL.

1423   i) Difference between CTL and observations for SST (in °C, contour interval: 0.25°C)

1424   calculated between April 15th and May 15th.

1425

1426   **Figure 5**:

1427   a) Lag-composite of 20-80 days filtered daily rainfall anomalies with a Lanczos filter

1428   (Duchon, 1979) (in mm/day, contour interval: 0.2mm/day) over a 60 days windows centered

1429   over the ISM onset. For each year, the 30 days preceding and the 30 days following the onset date,

1430   estimated as the day when the TTG index changes sign (Xavier et al. 2007), are selected. The daily

1431   average for each day of this 61 days time period is then calculated and averaged between 50°E

1432 and 90°E. The precipitations are estimated from TRMM.

1433   b) Same as a) but for FOR.

1434   c) Same as a) but for TRD.

1435

1436 **Figure 6**:

1437 Same as figure 2, but for the vertical shear of zonal wind (difference between zonal wind at 200

1438 and 850 hPa, units: m/s, contour interval: 5m/s for panel a and 1m/s for panels b and c) and the

1439 specific humidity at 850 hPa (units: kg/kg, contour interval: 0.0005kg/kg for panel d and

1440 0.0004kg/kg for panels e and f).

1441 The observed winds and specific humidity are estimated from ERA interim.

1442

1443 **Figure 7**:

1444   a) Map of correlation between the skin temperature (land surface temperature over the

1445   continent, SST over the ocean) averaged between April 15th and May 15th correlated with

1446   the onset date annual time series, for observations. The skin temperature and the onset

1447   date are estimated from ERAI. Contours show the area where correlation is significant at

1448   the 90% confidence level according to a two-tailed Student t test.

1449   b) Same as a), but for FOR.

1450   c) Same as a), but for CTL.

1451   d) Same as a) but for the TT estimated from ERAI.

1452   e) Same as d), but for FOR.

1453   f) Same as d), but for CTL.

1454   g) Same as a) but for the vertical shear of zonal wind (difference between zonal wind at 200

1455   and 850 hPa) estimated from ERAI.

1456   h) Same as g), but for FOR.

1457   i) Same as g), but for CTL.

1458

1459 **Figure 8**:

1460 a) Lead-lag correlation between the onset date and the Niño3.4 monthly time series (SST average

1461 between 190°-240°E and 5°N-5°S). Between January one year and a half before the monsoon

1462 onset and December one year and a half after the monsoon onset

1463   b) Same as a) for the IOB monthly time series (SST average between 40°-110°E and 20°N-20°S).

1464   For both figures, diamonds indicate when the correlation coefficient is significant at the 90%

1465   confidence level according to a two-tailed Student t test. Observations, estimated from ERAI are

1466   shown in black, FOR is shown in light blue and CTL is shown in red.

1467

1468   **Figure 9**:

1469   a) Running lead-lag correlations between the onset date and the vertical zonal wind shear index

1470   (zonal wind at 200 hPa minus wind at 850 hPa, in the region 60°E-90°E; equator-30°N) daily

1471   running mean over 30 days. The correlation is calculated between the onset date and the running

1472   means and is plotted at the central value of the running window. Vertical lines show the onset

1473   date. Crosses show the point where the correlation is above the 90% confidence level.

1474   b) As in a), but for lead-lag correlation between the onset date and rainfall over the northwest

1475   Pacific (120°-150°E and 0°-20°N).

1476   c)   Lead-lag correlation between the TT averaged between April 15th and May 15th in the

1477   northern box (40°-100°E; 5°- 35°N) and the Niño 3.4 monthly time series (SST average between

1478   190°-240°E and 5°N-5°S). Diamonds indicate when the correlation coefficient is significant at the

1479   90% confidence level according to a two-tailed Student t test.

1480   For all figures, Observations, estimated from ERAI are shown in black, FOR is shown in light blue

1481   and CTL is shown in red.

1482

1483

1484   **Figure 10**:

1485   Box plots of the onset date time series in observations and all experiments. From left to right,

1486   observations, FOR, CTL, FTIO, FTA, FTP and FTPC (color labeling in the figure). For each box plot,

1487   the bottom value represents the minimum of the empirical distribution, the upper value the

1488   maximum, then from bottom to top, the first horizontal line represents the first quartile, the cross

1489   represents the mean, the second line represents the median and the upper line represents the

1490   third quartile.

1491

1492

1493   **Figure 11**:

a)   Annual cycle of daily TTG (Tropospheric Temperature Gradient, in K) defined as the difference of the TT (Tropospheric Temperature; temperature averaged between 600 and 200 hPa) averaged in a northern box (40°-100°E; 5°- 35°N) and a southern box (40°-100°E; 15°S-5°N).

b)   Annual cycle of the daily TT (in K) averaged in the northern box (40°-100°E; 5°-35°N).

c)   Annual cycle of the daily TT (in K) averaged in the southern box (40°-100°E; 15°S-5°N).

Observations are shown in black (TT is derived from ERAI). Coupled and forced experiments are shown in red and light blue, respectively. FTA, FTIO, FTP and FTPC are shown in orange, green, dark blue and purple, respectively.

Figure 12:

a) Time-latitude diagram of daily climatology of precipitations (in mm/day, contour interval: 1.5mm/day) averaged between 50°-90°E, between March 1st and June 30th in CTL.

b) same as a), but for FTIO.

c) same as a), but for FTA.

d) same as a), but for FTP.

Figure 13:

a)   Difference between the SST averaged between April 15th and May 15th in FTP and CTL (units: °C, contour interval: 0.25°C). Contours show the area where the difference is above the 90% confidence level.

b)   Same as a) for the TT (units: °C, contour interval: 0.25°C).

c)   Difference between precipitations (shaded, units: mm/day, contour interval: 1mm/day) and 850 hPa winds (arrows, units: m/s) averaged between April 15th and May 15th in FTP and CTL. For winds, only the values significant at the 90% confidence levels are shown; for precipitations values below 90% confidence level are masked.

d)   Same as c) for vertical velocity (shaded, units: Pa/s, contour interval: 0.01Pa/s, upward motion are represented by negative values) and 200 hPa winds (arrows, units: m/s).

1525   e)   Same as a) for vertical shear of zonal wind (difference between zonal wind at 200

1526   and 850 hPa, units: m/s, contour interval: 1m/s).

1527   f)   Same as a) for humidity at 850 hPa (units: kg/kg, contour interval: 0.0004kg/kg).

1528

1529

1530   **Figure 14**:

1531   a)   Difference between the SST averaged between April 15th and May 15th in FTIO and

1532   CTL (units: °C, contour interval: 0.25°C). Contours show the area where the difference is

1533   above the 90% confidence level.

1534   b)   Same as a) for FTA.

1535   c)   Difference between the precipitation (shaded, units: mm/day, coutour interval:

1536   1mm/day) and 850 hPa winds (arrows, units: m/s) averaged between April 15th and May

1537   15th in FTP and CTL. For winds, only the values 90% significant are shown, for

1538   precipitations values under 90% of significance are masked.

1539   d)   Same as c) for FTA.

1540

1541

1542   **Figure 15**:

1543   a) Difference between the vertical shear of zonal wind (difference between zonal winds at

1544   200 and 850 hPa, units: m/s, contour interval: 1m/s) between April 15th and May 15th in

1545   FTIO and CTL. Contours show the area where the difference is above 90% confidence level.

1546   b) Same as a) for humidity at 850 hPa (units: kg/kg, contour interval: 0.0004 m/s).

1547

Figure 1

a) Precip
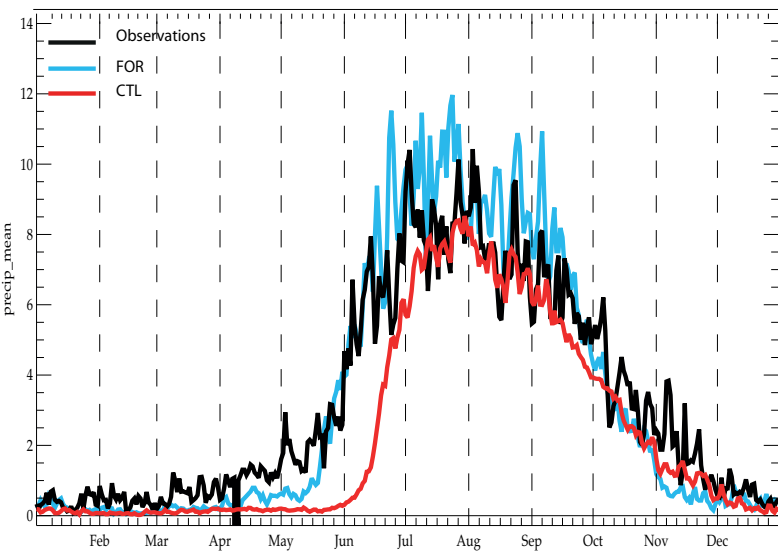
b) TTG
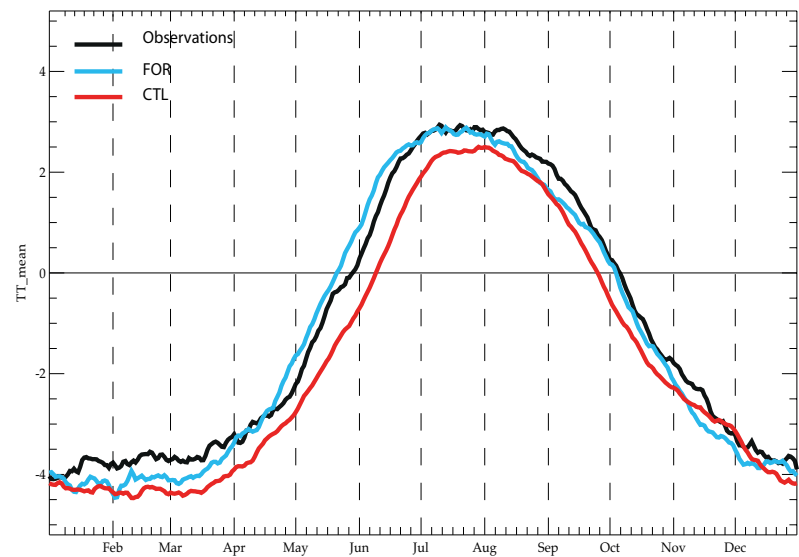
c) TT north
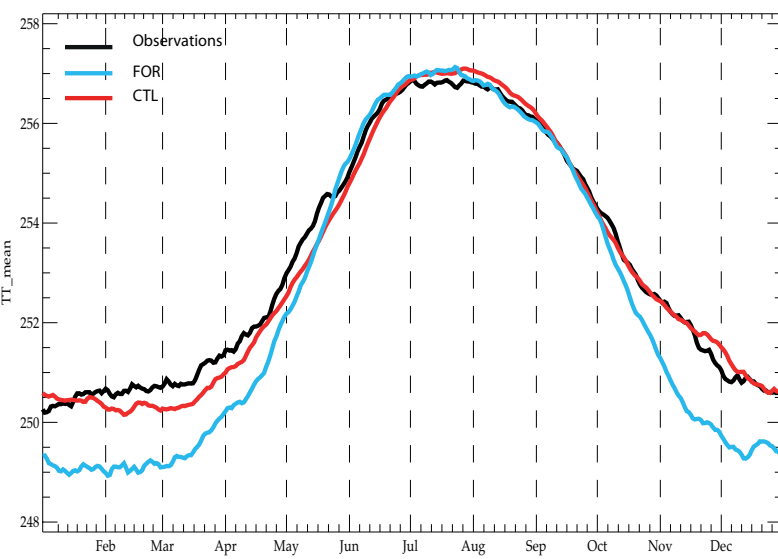
d) TT south
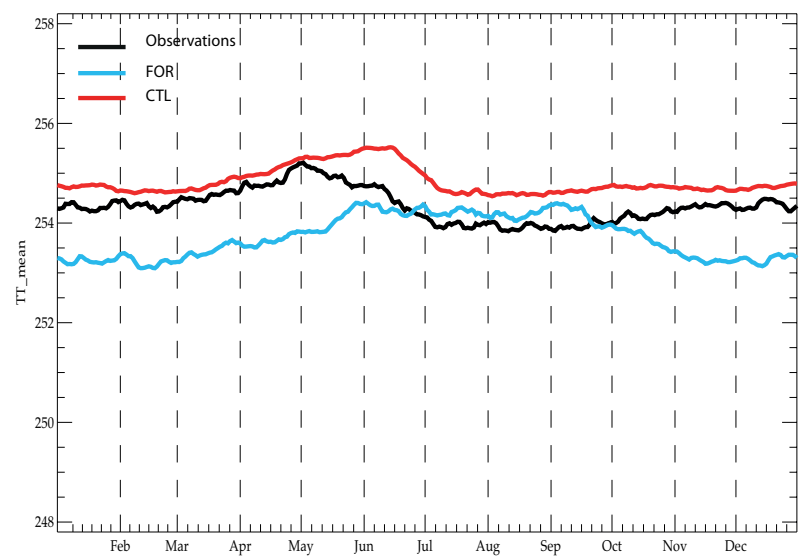
Figure 2

a) Obs: T2m
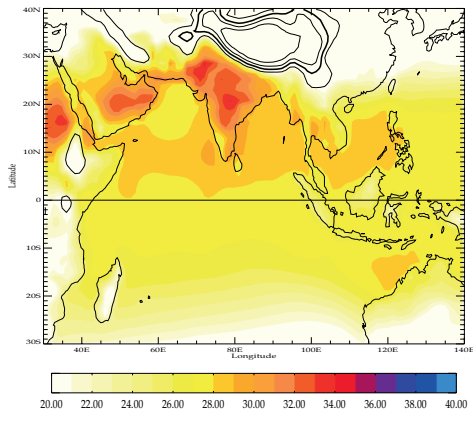
b) FOR-Obs: T2m
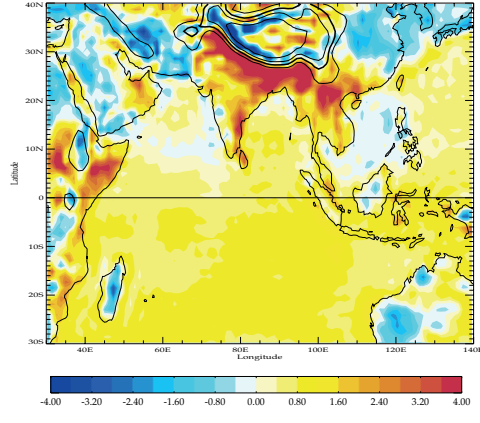
c) CTL-Obs: T2m
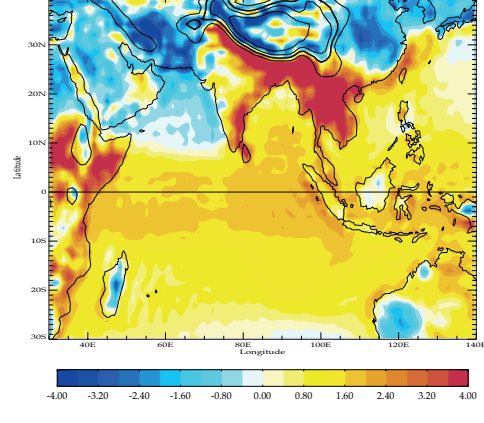
d) Obs: TT
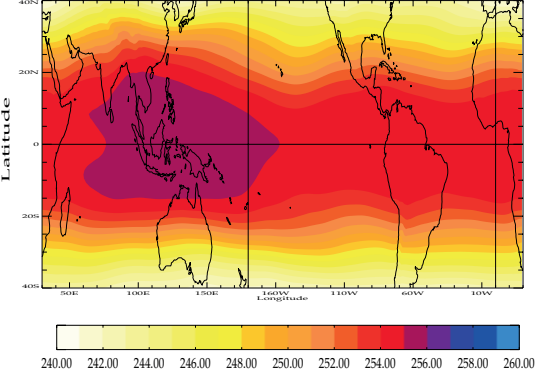
e) FOR-Obs: TT
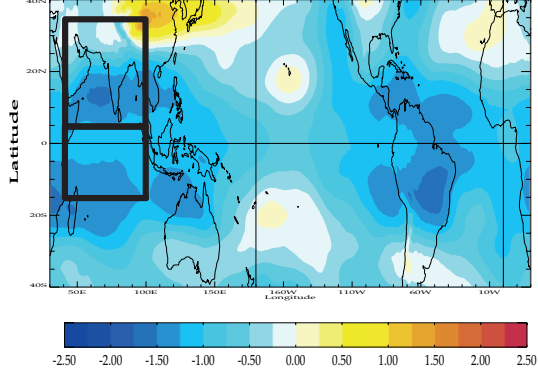
f) CTL-Obs: TT
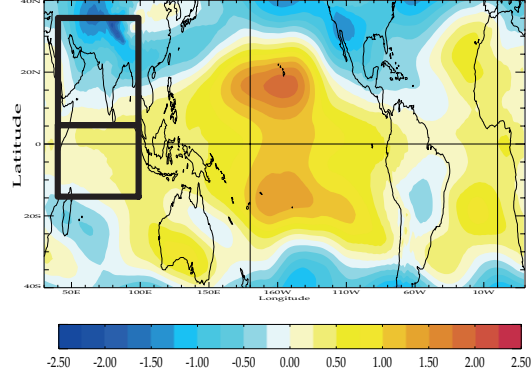
Figure 3

a) Observation: Precip   b) FOR: Precip   c) CTL: Precip

0.00 1.50 3.00 4.50 6.00 7.50 9.00 10.50 12.00 13.50 15.00

d) Observation: TT   e) FOR: TT   f) CTL: TT

250.00 251.00 252.00 253.00 254.00 255.00 256.00 257.00 258.00 259.00 260.00
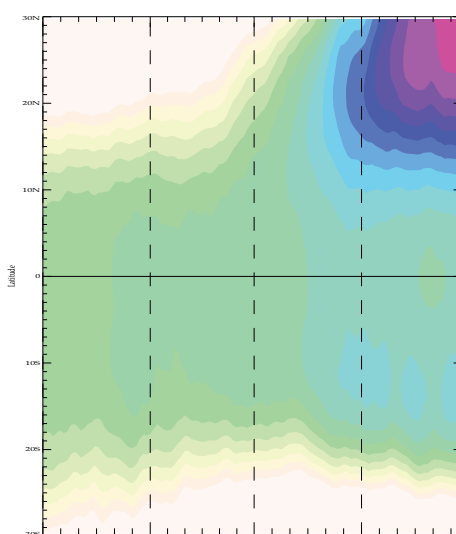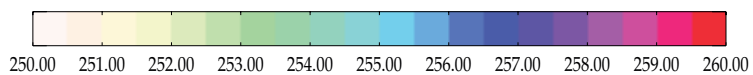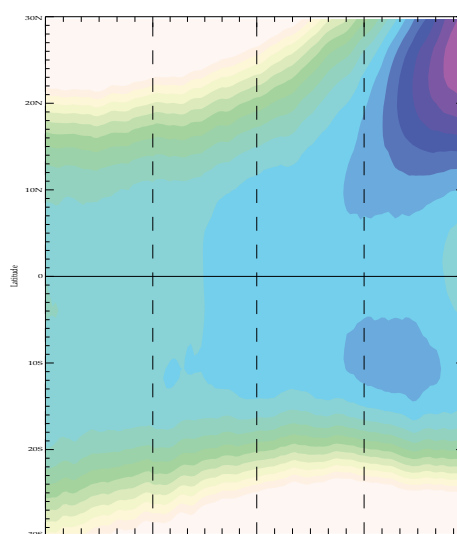
g) Observation: wind shear   h) FOR: wind shear   i) CTL: wind shear
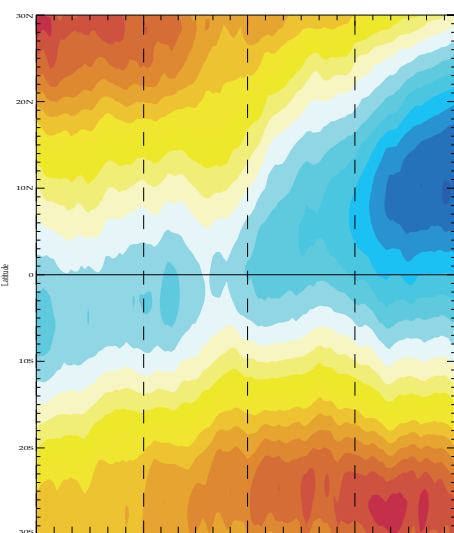
-50.00 -40.00 -30.00 -20.00 -10.00 0.00 10.00 20.00 30.00 40.00 50.00

Figure 4

a) Observation: precip & 850 hPa wind

b) FOR: precip & 850 hPa wind

c) CTL: precip & 850 hPa wind

d) CTL-FOR: precip & 850 hPa wind

e) FOR-Obs: precip & 850 hPa wind

f) CTL-Obs: precip & 850 hPa wind

g) Observation: SST

h) CTL: SST

i) CTL-Obs: SST

Figure 5

a) Observation: Precip

b) FOR: Precip

c) CTL: Precip

-2.00   -1.60   -1.20   -0.80   -0.40   0.00   0.40   0.80   1.20   1.60   2.00

Figure 6

a) Observation: ushear   b) FOR-obs: ushear   c) CTL-obs: ushear

d) Observation: q850   e) FOR-obs: q850   f) CTL-obs: q850

Figure 7

a) Observation: tsurf   b) FOR: tsurf   c) CTL: tsurf

d) Observation: TT   e) FOR: TT   f) CTL: TT

g) Observation: ushear   h) FOR: ushear   i) CTL: ushear

Figure 8

a) lead-lag cor: onset date & Nino 3
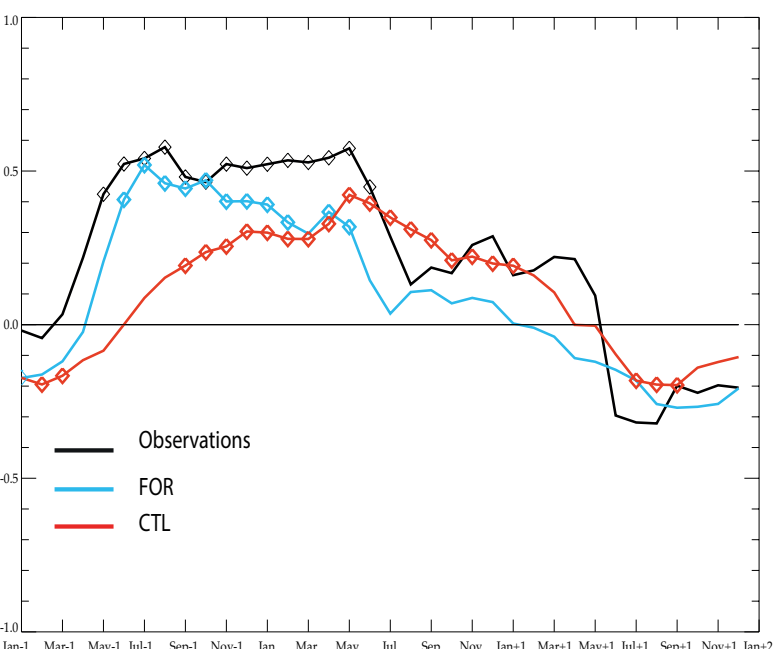
b) lead-lag cor: onset date & IOB

Figure 9

a) lead-lag cor: onset date & ushear

b) lead-lag cor: onset date & precip

c) lead-lag cor: Northern TT & Nino 3.4

Figure 10

Figure 11

a) TTG

b) Northern TT

c) Southern TT

Figure 12

a) CTL: Precip

b) FTIO: Precip

c) FTA: Precip

c) FTP: Precip
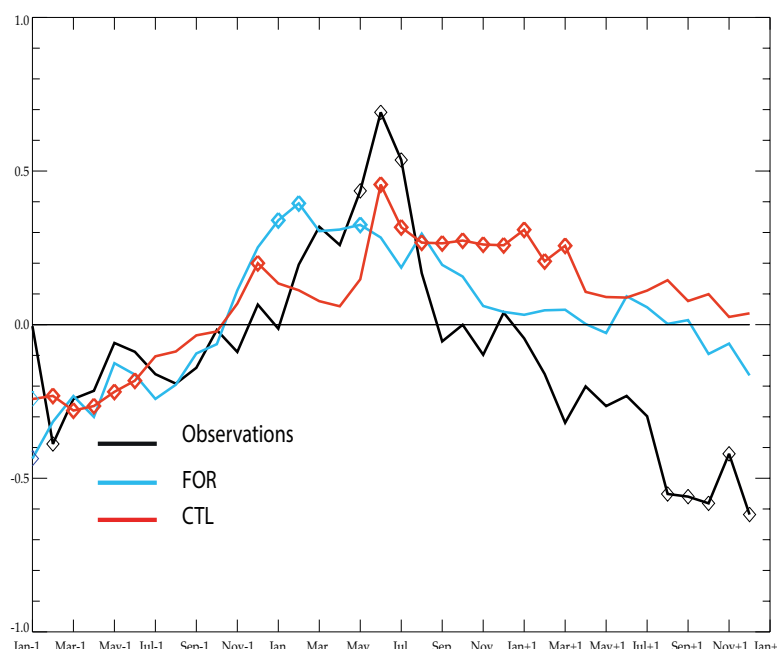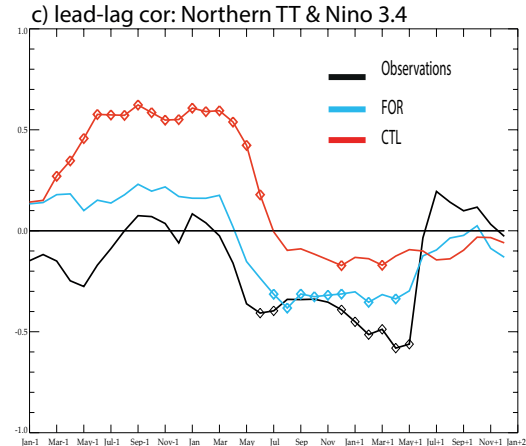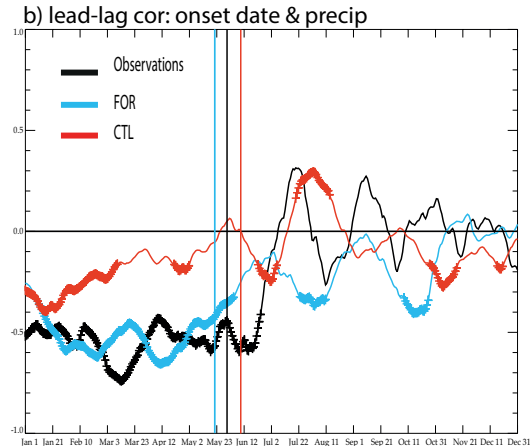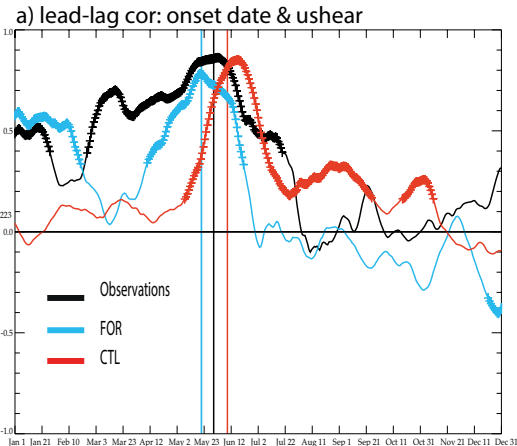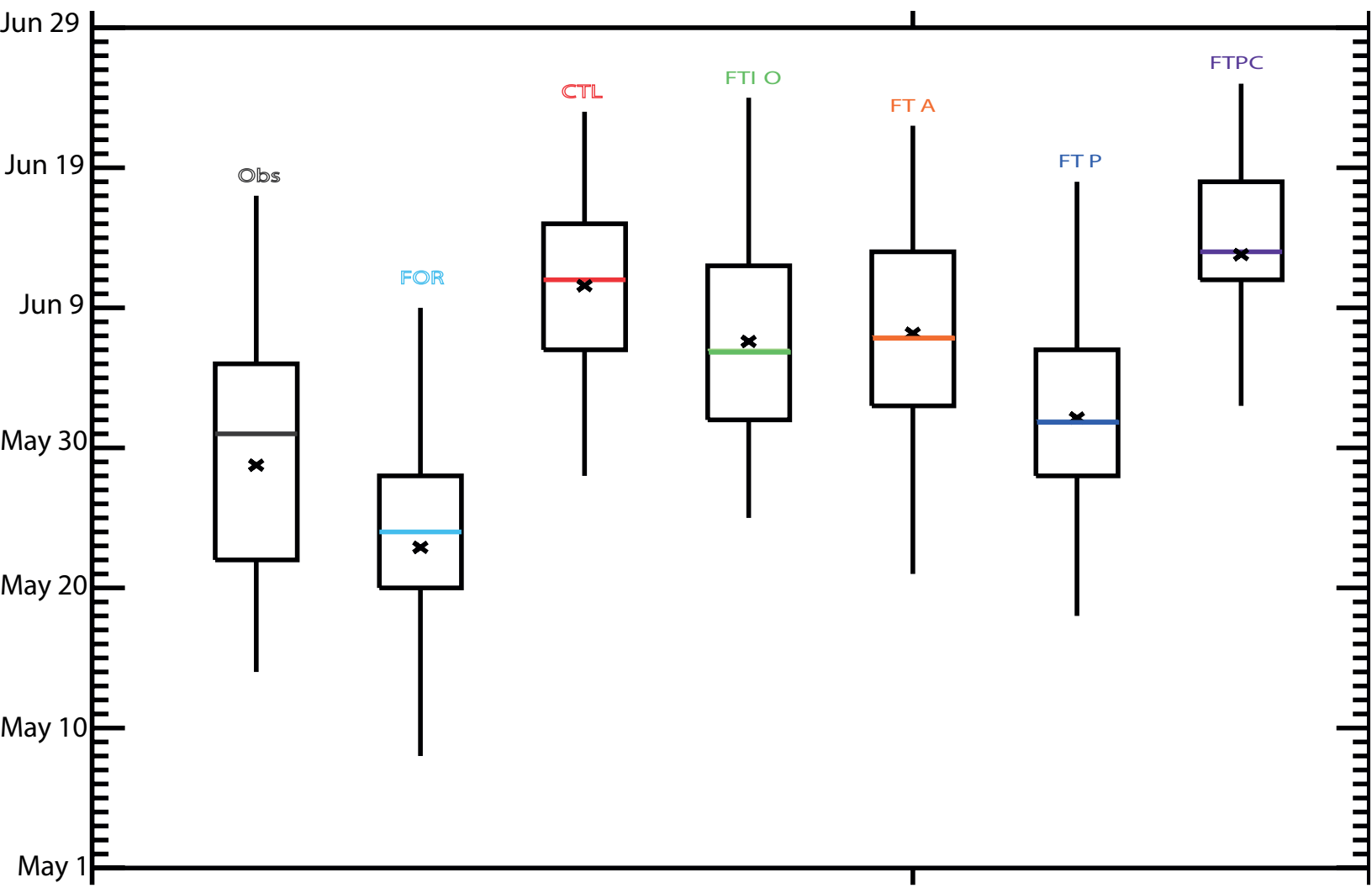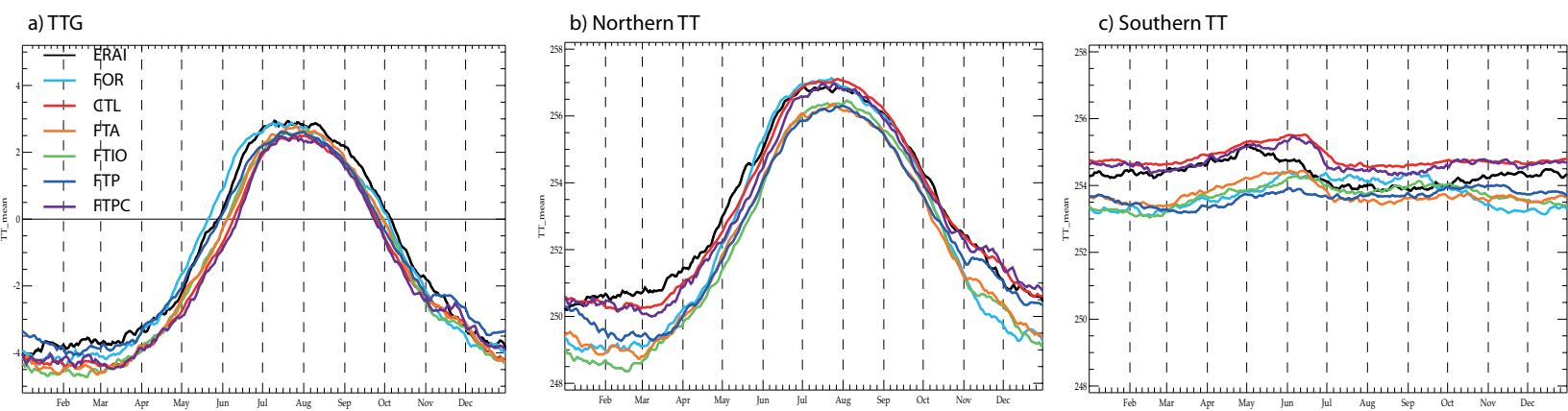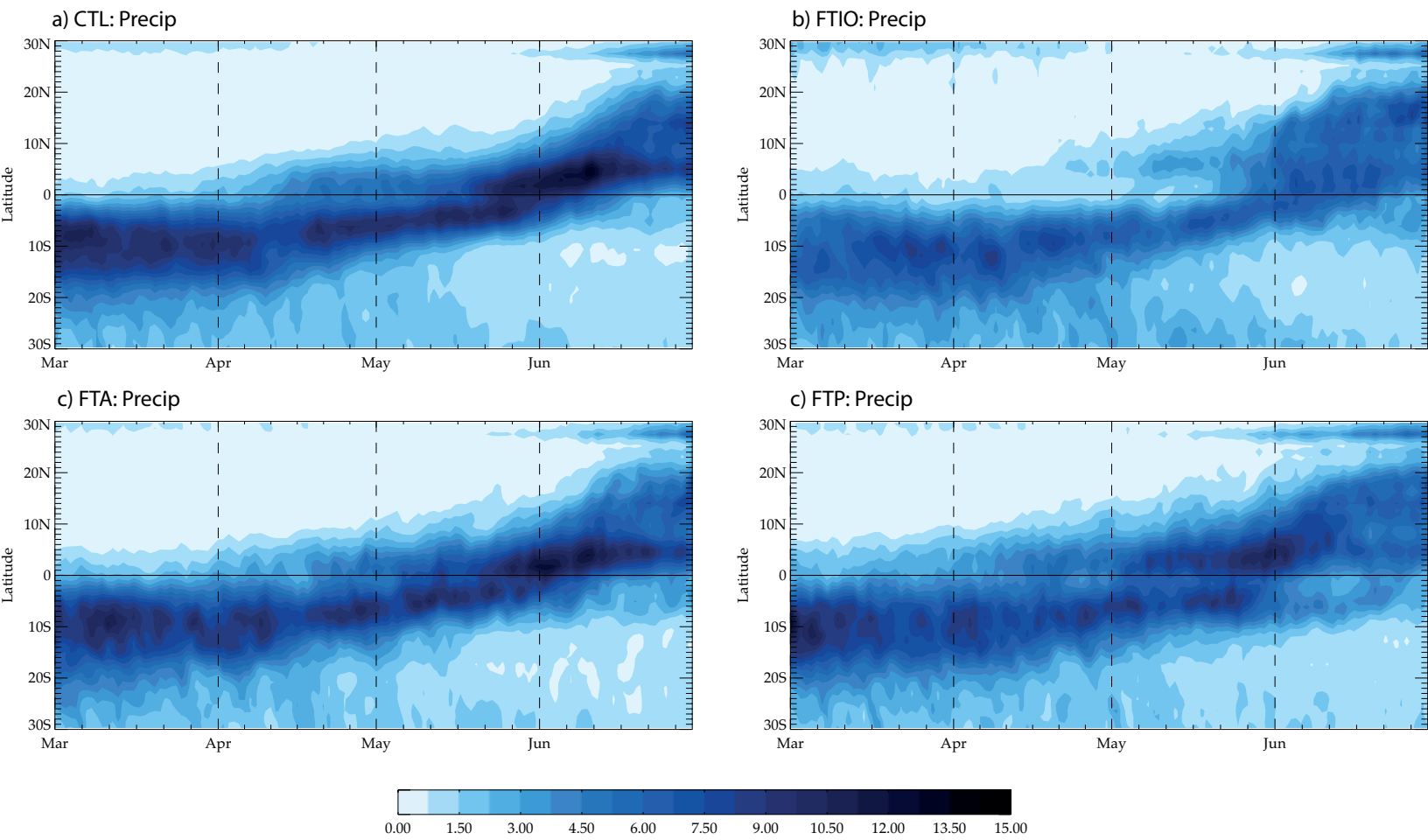
Figure 13
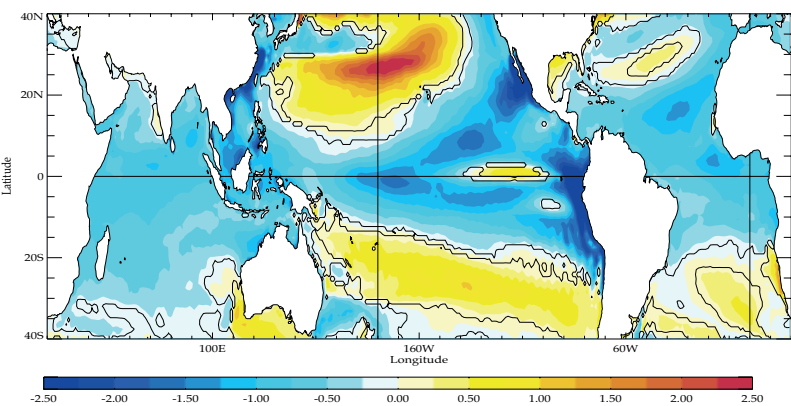
a) FTP-CTL: SST

b) FTP-CTL: TT
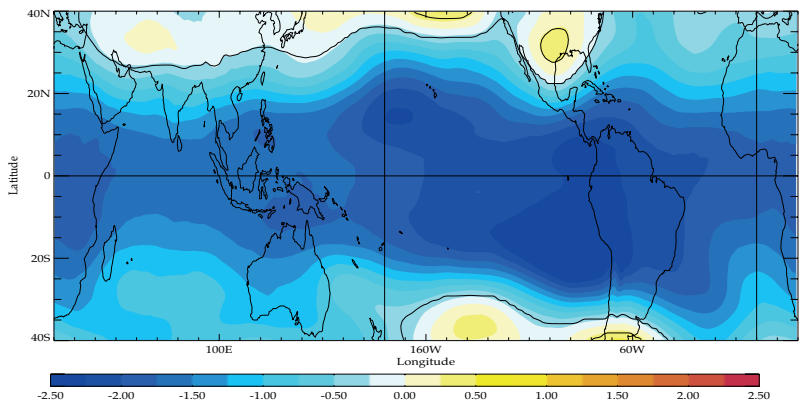
c) FTP-CTL: precip & 850hPa winds
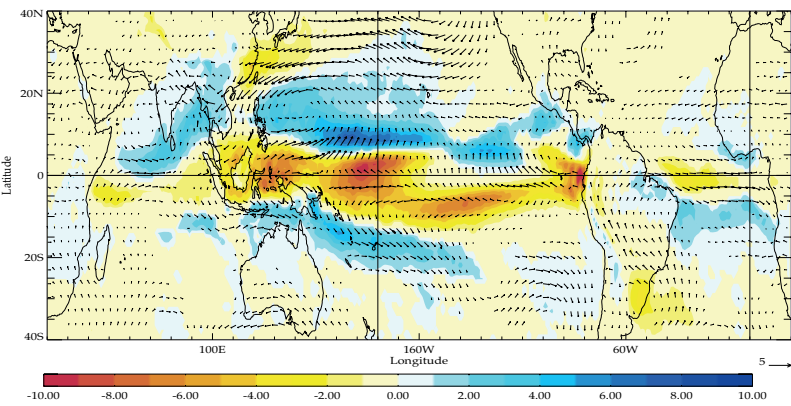
d) FTP-CTL: omega500 & 200hPa winds
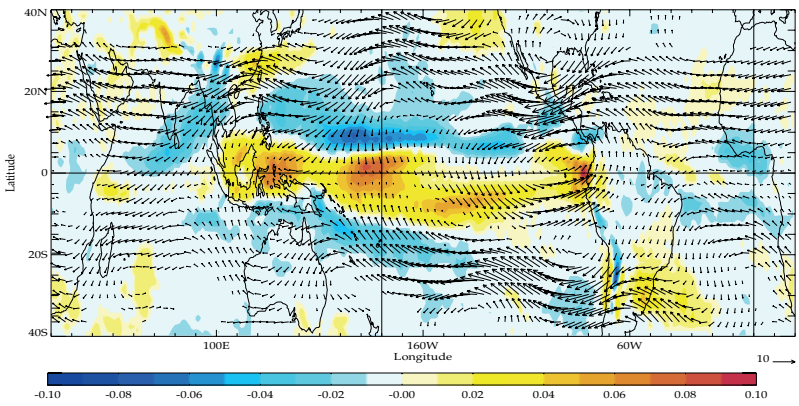
e) FTP-CTL: ushear
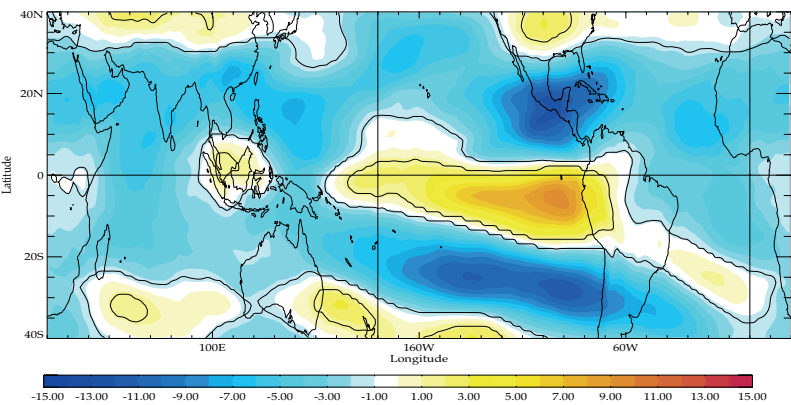
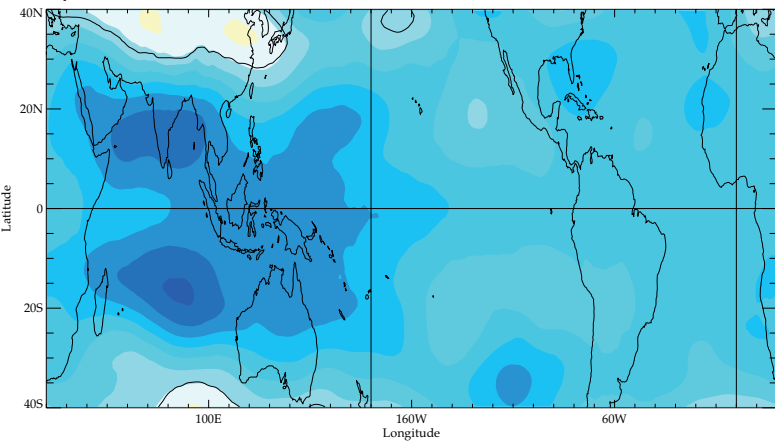f) FTP-CTL: q850
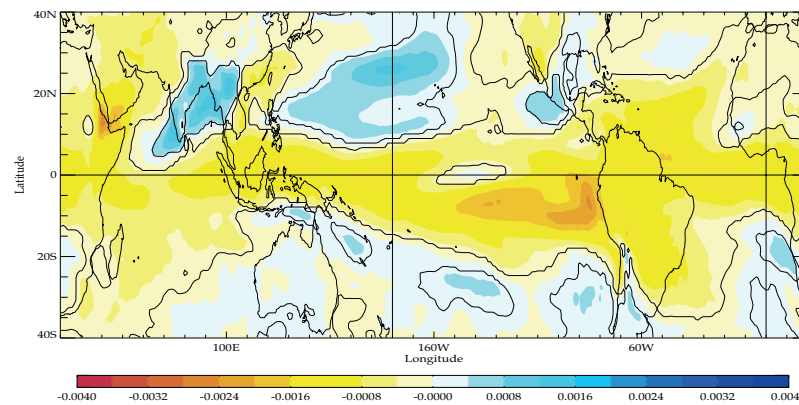
Figure 14

a) FTIO-CTL: SST
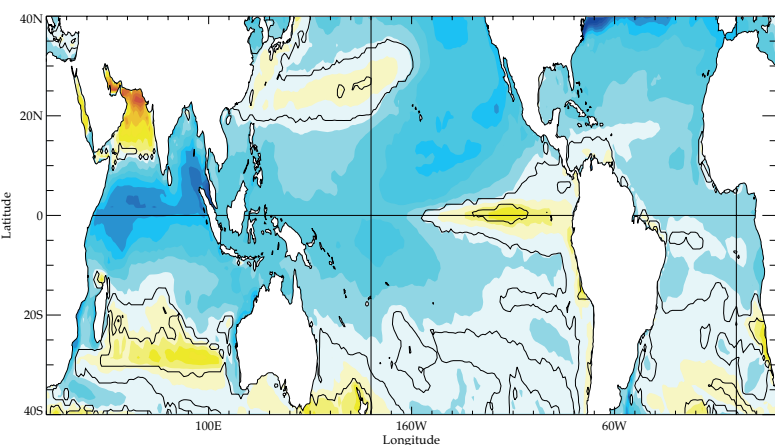
b) FTA-CTL: SST
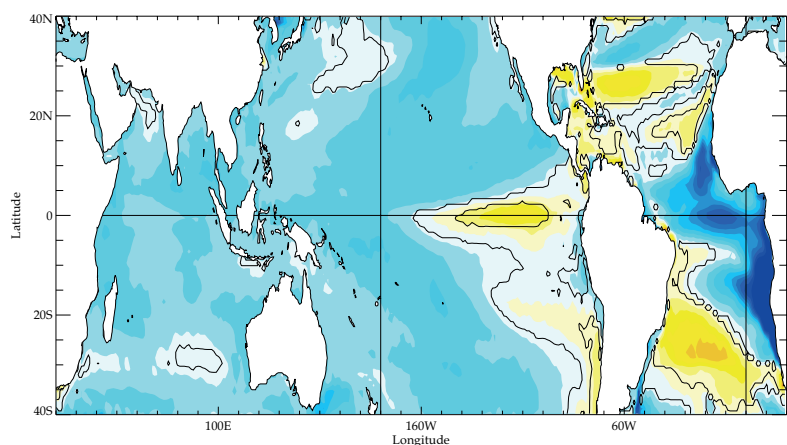
c) FTIO-CTL: precip & 850hPa winds
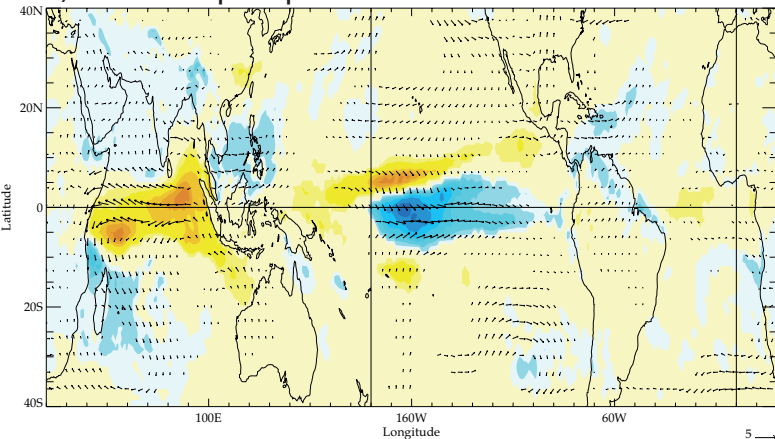
d) FTA-CTL: precip & 850hPa winds
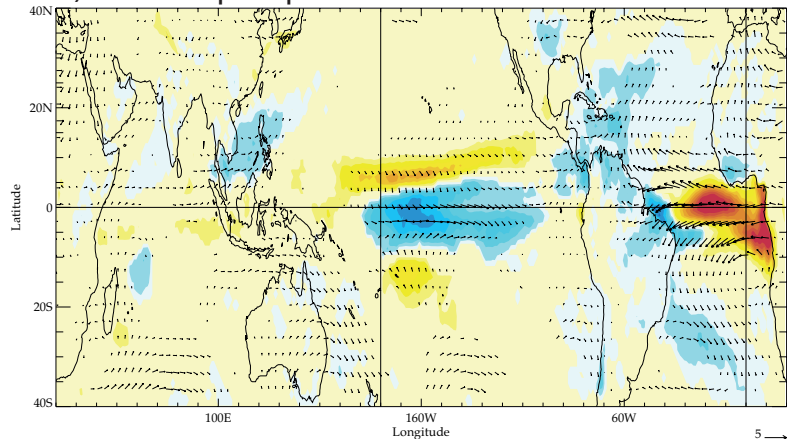
e) FTIO-CTL: TT

f) FTA-CTL: TT

Figure 15
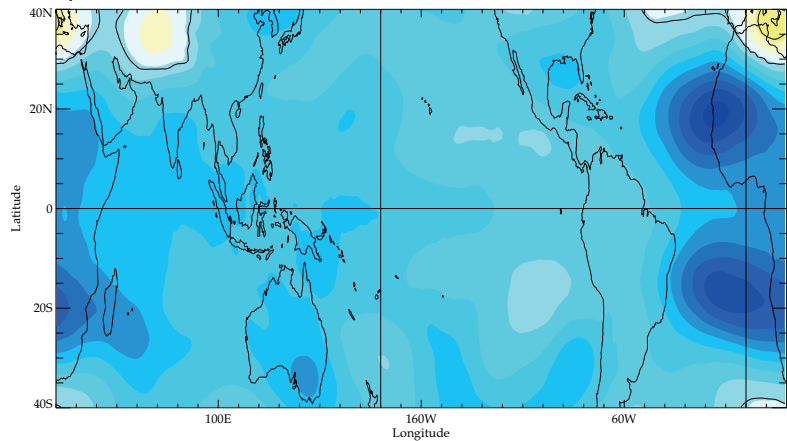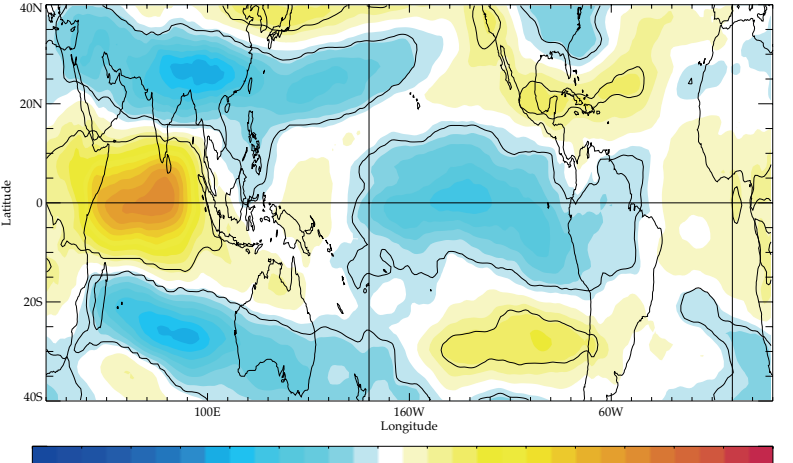
a) FTIO-CTL: ushear

b) FTIO-CTL: q850